Cell Reports

Article

A developmental critical period for ocular dominance plasticity of binocular neurons in mouse superior colliculus

Graphical abstract

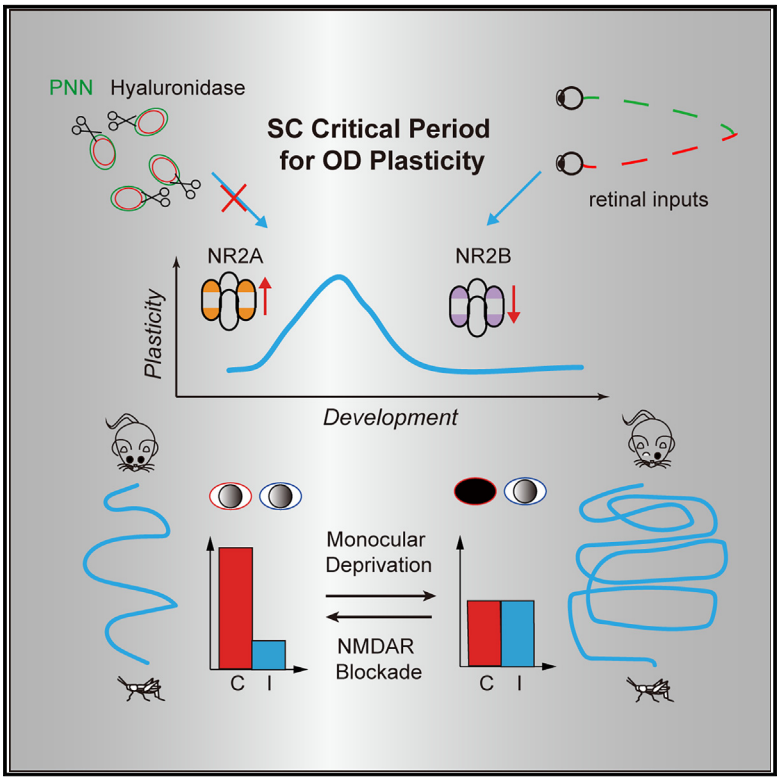

Authors

Guanglei Hu, Ailin Chen, Jingjing Ye, ..., Menghan Dai, Xuefeng Shi, Yu Gu

Correspondence

shixf_tmu@163.com (X.S.), guyu_@fudan.edu.cn (Y.G.)

In brief

Hu et al. uncover the critical period for OD plasticity in mouse SC, which is similar to, but independent of, V1 and requires SC NMDA receptors. Predatory impairments caused by MD can be prevented by NMDA receptor blockade, suggesting the pivotal role of subcortical visual circuitry in amblyopia.

Highlights

- A developmental critical period for OD plasticity exists in mouse SC binocular neurons
- SC OD plasticity is independent of V1 inputs
- SC OD plasticity requires NMDA receptors
- The predatory impairments caused by MD can be prevented by NMDA receptor blockade

Hu et al., 2024, Cell Reports *43*, 113667
January 23, 2024
https://doi.org/10.1016/j.celrep.2023.113667

CellPress

Cell Reports

CellPress
OPEN ACCESS

Article

A developmental critical period for ocular dominance plasticity of binocular neurons in mouse superior colliculus

Guanglei Hu,[1,4,8] Ailin Chen,[2,8] Jingjing Ye,[2,3] Qiong Liu,[4] Jiafeng Wang,[2] Cunxiu Fan,[5] Xiaoqing Wang,[6] Mengqi Huang,[1] Menghan Dai,[1] Xuefeng Shi,[2,3,7,*] and Yu Gu[1,9,*]

[1]State Key Laboratory of Medical Neurobiology and MOE Frontiers Center for Brain Science, Institutes of Brain Science, Fudan University, Shanghai 200032, China

[2]Tianjin Eye Hospital, Tianjin Key Laboratory of Ophthalmology and Visual Science, Tianjin Eye Institute, Clinical College of Ophthalmology, Tianjin Medical University, Tianjin 300020, China

[3]Medical College of Optometry and Ophthalmology, Shandong University of Traditional Chinese Medicine, Jinan 250014, China

[4]School of Life Sciences, Westlake University, Hangzhou 310000, China

[5]Jiading Branch of Shanghai General Hospital, Shanghai Jiao Tong University School of Medicine, 800 Huangjiahuayuan Road, Shanghai 201803, China

[6]Department of Dermatology, Shanghai Ninth People's Hospital, Shanghai Jiao Tong University School of Medicine, Shanghai 200011, China

[7]Institute of Ophthalmology, Nankai University, Tianjin 300020, China

[8]These authors contributed equally

[9]Lead contact

*Correspondence: shixf_tmu@163.com (X.S.), guyu_@fudan.edu.cn (Y.G.)

https://doi.org/10.1016/j.celrep.2023.113667

SUMMARY

Detecting visual features in the environment is crucial for animals' survival. The superior colliculus (SC) is implicated in motion detection and processing, whereas how the SC integrates visual inputs from the two eyes remains unclear. Using *in vivo* electrophysiology, we show that mouse SC contains many binocular neurons that display robust ocular dominance (OD) plasticity in a critical period during early development, which is similar to, but not dependent on, the primary visual cortex. NR2A- and NR2B-containing N-methyl-D-aspartate (NMDA) receptors play an essential role in the regulation of SC plasticity. Blocking NMDA receptors can largely prevent the impairment of predatory hunting caused by monocular deprivation, indicating that maintaining the binocularity of SC neurons is required for efficient hunting behavior. Together, our studies reveal the existence and function of OD plasticity in SC, which broadens our understanding of the development of subcortical visual circuitry relating to motion detection and predatory hunting.

INTRODUCTION

During early postnatal development, ocular dominance (OD) plasticity in the primary visual cortex (V1) is one of the most thoroughly studied and well-characterized models for experience-dependent refinement of the circuital and synaptic plasticity.[1,2] In carnivores and primates, OD plasticity is confined to a specific time window called the critical period,[3–5] whereas in mice, OD shifts can be induced in the binocular zone of the V1 for a short duration of monocular deprivation (MD) in juveniles and for a long duration in adults.[5,6] During the past half century, the underlying mechanism of V1 OD plasticity has been well illustrated. According to the prevailing view, OD plasticity is considered to occur exclusively at the cortical level,[7,8] which is absent in subcortical visual areas such as the dorsal lateral geniculate nucleus (dLGN).[9–12] However, this dogma has been challenged by recent works indicating that the dLGN does express OD plasticity.[13–16] MD during early development shifts the relative contralateral and ipsilateral responses of thalamocortical neurons, which requires the expression of the $GABA_A$ receptor $\alpha 1$ subunit.[14]

The superior colliculus (SC) is a mammalian homolog of the optic tectum, a major retinofugal target and vision processing center, as well as an evolutionarily conserved midbrain structure for multimodal integration[17,18] and sensorimotor transformation.[19–22] Although the SC has long been held as a sensory information integrator responsible for the initiation of eye and head movement toward visual targets,[23,24] it was largely neglected in the study of OD plasticity. Approximately 80% dLGN-projecting retinal ganglion cells (RGCs) also send axon collateral to the SC, which could provide a neural basis for binocular responses and competitive OD plasticity in the SC.[13,25] While a series of studies have reported functional and structural plasticity in the optic tectum of tadpole Xenopus, which forms binocular vision through a very different pathway that is not direct from the retina,[26–29] few investigations have been performed on the OD plasticity of mammalian SC.

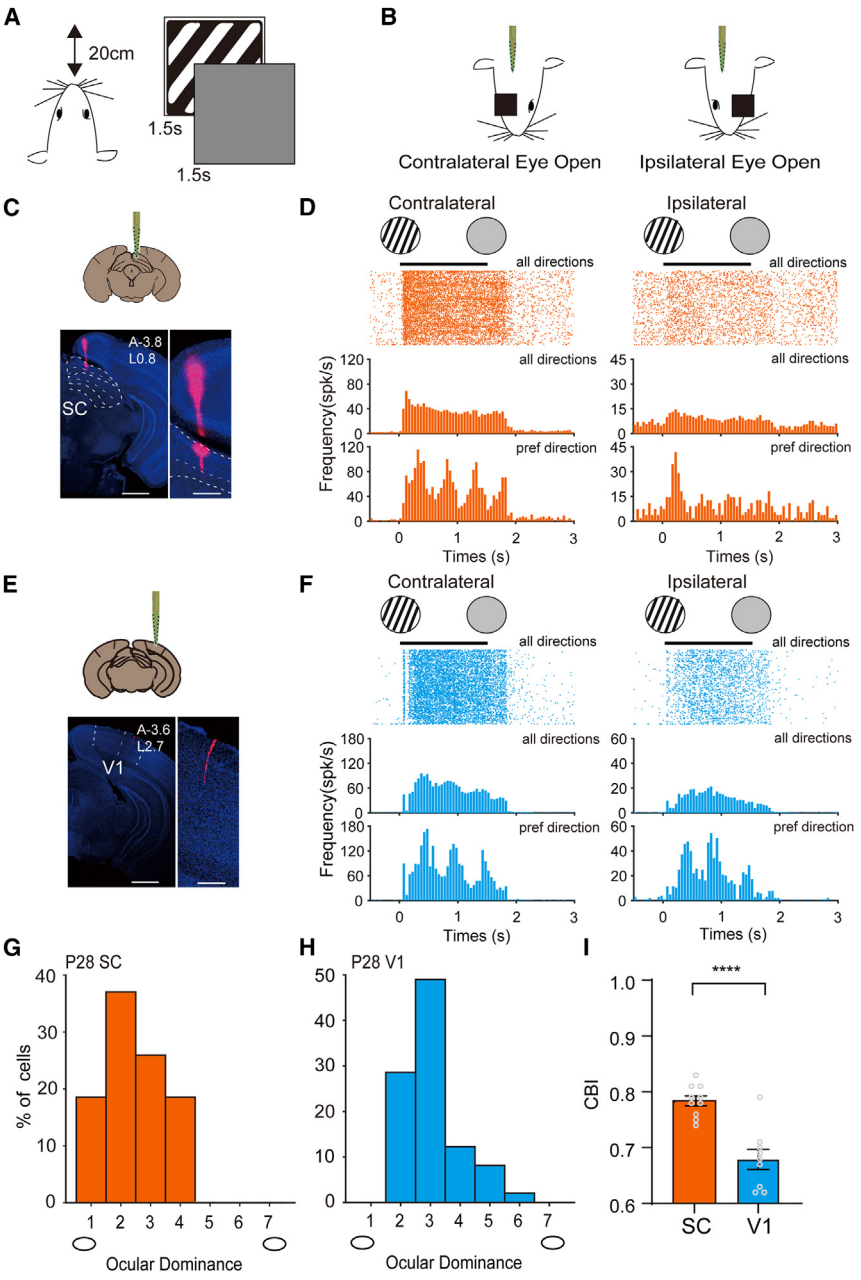

Figure 1. SC shows a stronger contralateral bias than V1

(A) Schematic of visual stimulus paradigm.

(B) Schematic of eye specificity (contralateral and ipsilateral) in which visual stimuli were presented.

(C) Top: typical location of electrodes in SC of an example mouse, superimposed on "The Mouse Brain." Bottom left: a coronal section showing electrode track in the SC. The electrode was dipped with a lipophilic dye (DiI, 1,1′-dioctadecyl-3,3,3′, 3′-tetramethylindocarbocyanine perchlorate), allowing post hoc visualization of the electrode's path; the borders and layers of the SC are demarcated with dashed white lines. Scale bar, 1,000 μm. Bottom right: locally enlarged image showing the detail of the electrode track. Scale bar, 300 μm.

(D) Examples of spike raster plots (for all directions) and peristimulus time histograms (PSTHs, for all directions and preferred direction) of an SC neuron in response to full-field drifting grating with contralateral (left) and ipsilateral eye (right). Solid lines indicate 0–1.5 s after the onset of drifting grating stimulation.

(E) Top: schematic of recording site in binocular V1 of an example mouse, superimposed on "The Mouse Brain." Bottom left: a coronal section showing electrode track in the V1; the borders of the V1 are demarcated with dashed white lines. Scale bar, 1,000 μm. Bottom right: locally enlarged image showing the detail of the electrode track. Scale bar, 300 μm.

(F) Examples of spike raster plots (for all directions) and PSTHs (for all directions and preferred direction) of a V1 neuron in response to full-field drifting grating with contralateral (left) and ipsilateral eye (right).

(G and H) Distribution of OD scores for SC (G, 461 cells from 9 mice) and V1 (488 cells from 10 mice) of normal P28 mice.

(I) Mean CBIs for SC and V1 of normal P28 mice. Open circles represent individual CBIs for each animal. Data are presented as mean ± SEM. Mann-Whitney U test.

****$p < 0.0001$.

RESULTS

Binocular neurons in mouse SC showed a stronger contralateral bias than V1

To assess eye-specific responses to visual stimuli, we performed *in vivo* electrophysiological recordings with 16-channel silicon probes in the SC of anesthetized postnatal day 28 (P28) mice, in response to full-field drifting grating (1.5 s) applied at varying orientations to either eye (Figures 1A and 1B). Despite being dominated by the contralateral stimulation,[30] we observed that a great amount of visually responsive SC cells displayed binocular responses (Figures 1C, 1D, and S1G), which is largely consistent with a recently published study.[31] To compare the SC binocular neurons with the V1, we performed similar recordings in the V1 binocular zone (Figures 1E and 1F). We calculated the OD score from the binocular neurons of the SC and V1, which was quantitatively attributed to each neuron based on the response to

In the current study, using *in vivo* electrophysiology, we examined the OD plasticity in mouse SC. We found that pronounced OD shifts could be induced in SC binocular neurons with 4-day MD and that this plasticity was confined to a well-defined critical period. In addition, this subcortical plasticity was not due to corticofugal projection to SC. OD plasticity in SC was dependent on NMDA receptors, the blocking of which partially prevented the deficits of hunting efficiency after MD during the critical period. Together, our findings reveal that the visual experience-dependent maturation of subcortical sensory circuits directly affected the visually driven innate behavior, the detailed mechanism of which requires further investigation.

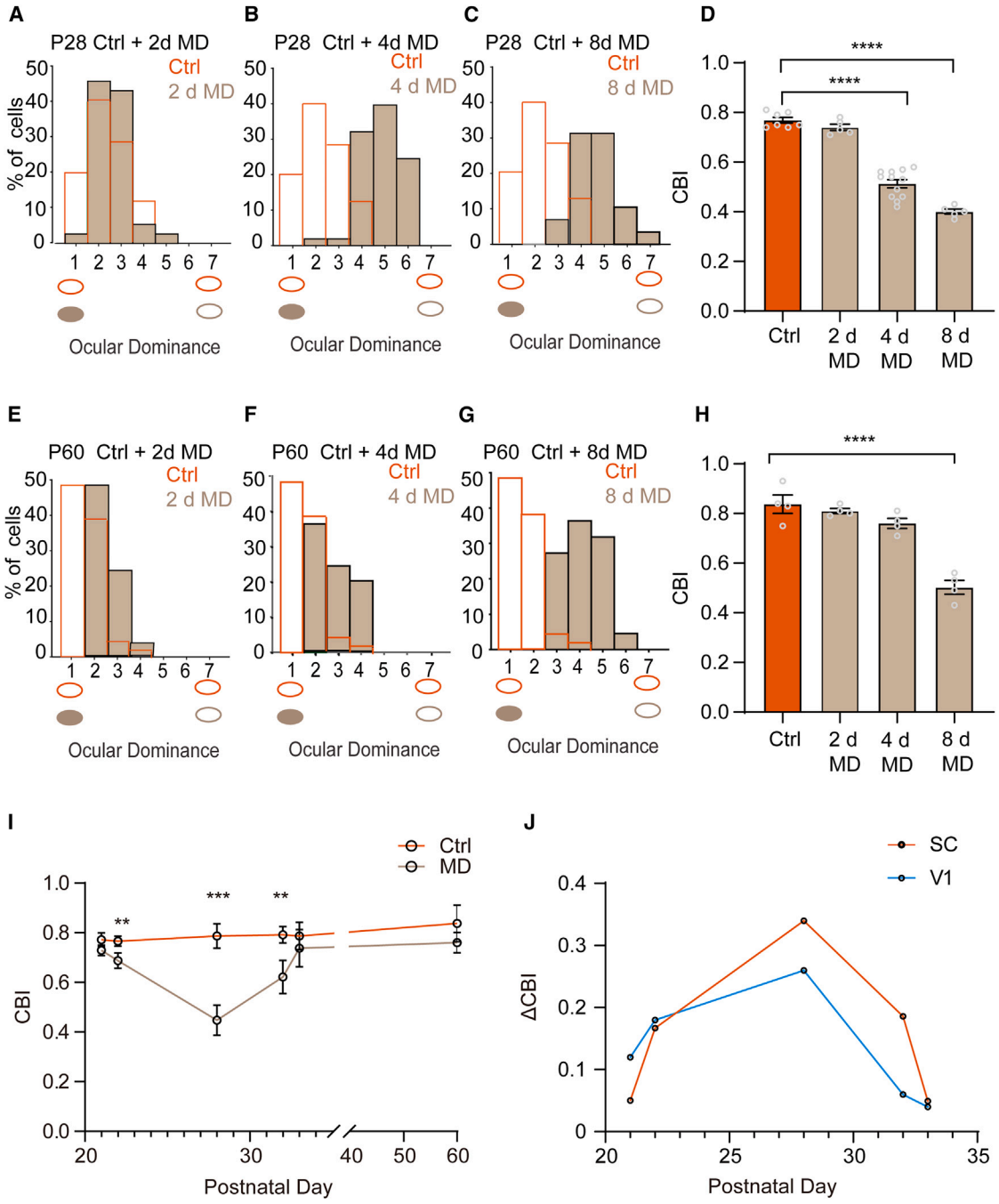

Figure 2. The critical period for OD plasticity in mouse SC

(A) Distribution of OD scores for SC from normal (246 cells from 7 mice) and 2-day MD mice (193 cells from 5 mice) starting at P28.

(B) Distribution of OD scores for SC from normal and 4-day MD mice (412 cells from 12 mice) starting at P28.

(C) Distribution of OD scores for SC from normal and 8-day MD mice (146 cells from 5 mice) starting at P28. Note that the age of the control mice is the same as the MD mice.

(D) Mean CBIs of all groups shown in (A)–(C). Open circles represent individual CBIs for each animal.

(E) Distribution of OD scores for SC from normal (203 cells from 4 mice) and 2-day MD mice (131 cells from 4 mice) starting at P60.

(F) Distribution of OD scores for SC from normal and 4-day MD mice (185 cells from 4 mice) starting at P60.

(G) Distribution of OD scores for SC from normal and 8-day MD mice (179 cells from 4 mice) starting at P60.

(H) Mean CBIs of all groups are shown in (E)–(G). Open circles represent individual CBIs for each animal.

(legend continued on next page)

visual stimulation of either eye, and the distribution of the OD score was summarized with the contralateral bias index (CBI). We found the V1 CBI value was consistent with previous literature (0.66 ± 0.03; Figures 1H and 1I).[5,32] Consistent with the results that only ~5% the anatomical inputs are ipsilateral in the SC,[30] we found that the SC exhibited a stronger contralateral bias than the V1 (0.79 ± 0.03; Figures 1G and 1I).

It is interesting to note that the binocular neurons in the SC we observed seemed more abundant than previously thought. To confirm that the binocular neurons we recorded are indeed binocular, and not due to artifacts such as light leakage, we performed a control experiment to occlude both eyes during the recording in the SC and V1. We found that with both eyes occluded, the visual responses dropped to zero, indicating that the eye occlusion method was valid and complete (Figures S1A–S1F). We also quantified all the neurons we recorded in the SC and revealed that the majority of the SC neurons were dominated by the contralateral input, and no ipsilateral-only responsive neurons were observed (Figure S1G), consistent with the literature.[18,30,33]

To better examine the location of the SC binocular neurons, we expanded our recording sites to cover the whole SC as much as we could and performed reconstruction of the electrode track with DiI staining after recording. Interestingly, we found that binocular responses can be recorded in the anterior, middle, and posterior portions of the SC and that they can also be recorded in both medial and lateral portions of the SC (Figure S2). For the whole SC, the localization of the binocular neurons almost spanned the whole SC, but generally speaking, the anterior SC showed a higher binocular neuron density compared to other regions of the SC (Figure S3). Therefore, we only included the anterior SC (Figure 1C) in the following analysis, which was considered as the binocular part of SC. And only the binocular SC neurons with clear contralateral and ipsilateral responses were analyzed (see STAR Methods for details).

A developmental critical period for OD plasticity existed in mouse SC binocular neurons

Since we recorded a large number of binocular neurons in mouse SC, it is interesting to ask if these SC binocular neurons are developmentally regulated by visual experience, similar to the V1.[5] To test this, we performed SC recordings in both normally reared and MD juvenile mice (P28). We found that 2-day MD had little effect (0.74 ± 0.04; Figures 2A and 2D), whereas 4- (0.51 ± 0.06) and 8-day MD (0.40 ± 0.01) starting at P28 significantly shifted the OD toward the ipsilateral eye, concurrent with a significant decline of CBI (Figures 2B–2D). Our findings revealed that extensive OD plasticity took place in mouse SC during early postnatal development.

It has been shown that the robust OD shift in juvenile V1 induced by brief MD (4 days) can still be elicited by longer periods of MD in adult mice.[6,34,35] To ask whether the same is true for the SC, we examined the effects of different periods of MD (2, 4, and 8 days) on the SC in adult mice (P60). Like in the V1, 8-day MD significantly shifted OD distribution in favor of the ipsilateral (open) eye (0.50 ± 0.06; Figures 2G and 2H), whereas brief 2- (0.81 ± 0.01) and 4-day MD (0.76 ± 0.04) did not significantly change the average CBI at this age (Figures 2E, 2F, and 2H).

Since we observed different effects of a brief, 4-day MD beginning at P28 and P60, we wanted to examine the developmental changes of SC OD plasticity and whether it was confined to a critical period like the V1.[5] To test this, we performed MD at the following ages, P21, P22, P28, P32, and P33, and did electrophysiological recordings 4 days later. We found that the maximal effects of MD were caused by 4-day MD starting at P28 (Figure 2I). A slight but significant shift toward the open ipsilateral eye was observed at P22 (Figures S4C and S4D), whereas at P21, the difference was not significant (Figures S4A and S4B). The magnitude and reliability of shifts induced by 4-day MD dropped rapidly after the peak of the period of susceptibility. MD at P32 can still induce a significant shift toward the ipsilateral eye (Figures S4E and S4F), whereas, at P33, there were no significant differences between MD and control animals (Figures S4G and S4H). The above results revealed a critical period for OD plasticity in the SC, which was largely in agreement with a previous report characterizing the critical period in the V1 (Figure 2J).[5]

Spine morphological transitions in SC showed similar developmental regulation to critical-period plasticity

Previous studies have shown that dendritic spine morphological transitions may provide a structural basis for synaptic plasticity.[36–39] To examine the developmental profile of dendritic protrusions in the SC, we used the fluorescent marker DiI to characterize the developmental alterations in the morphology of dendritic spines in SC slices. We qualified filopodia, stubby, thin, and mushroom spines according to their shape and size, as described previously (Figure 3A).[38,40] Similar to the trend observed in other brain regions, an age-related decline in dendritic spine abundance was observed in mouse SC (P13: 21.59 ± 1.14/10 μm, P28: 16.21 ± 0.53/10 μm, P60: 12.00 ± 0.75/10 μm; Figures 3B and 3C). Filopodial-type and thin spine densities at P60 were significantly lower than P13 and P28 (filopodial type: P13: 3.82 ± 0.49/10 μm, P28: 2.16 ± 0.40/10 μm, P60: 0.80 ± 0.21/10 μm; thin: P13: 5.84 ± 0.64/10 μm, P28: 4.64 ± 0.23/10 μm, P60: 2.49 ± 0.60/10 μm; Figures 3D and 3E), whereas stubby- and mushroom-type spine densities trended upward with age (stubby: P13: 1.00 ± 0.26/10 μm, P28: 2.36 ± 0.28/10 μm, P60: 3.24 ± 0.34/10 μm; mushroom: P13: 1.11 ± 0.18/10 μm, P28: 1.61 ± 0.27/10 μm, P60: 2.74 ± 0.15/10 μm; Figures 3F and 3G). These results demonstrated that developmental stages in the SC are accompanied by changes in spine morphology (Figure 3H).

We wonder if the changes of SC spine morphology with age are really associated with OD plasticity. To investigate how visual deprivation affects spine morphology in the SC, MD via eyelid

(I) Mean CBIs for normal (open circle) and 4-day MD mice (filled box) at various ages.
(J) Mean ΔCBI for SC (blue) and V1 (red) between Ctrl and 4-day MD mice at different ages.
Data are presented as mean ± SEM. One-way ANOVA with Tukey's post hoc test for (D) and (H) and unpaired two-sided t test for (I). **p < 0.01, ***p < 0.001, and ****p < 0.0001.

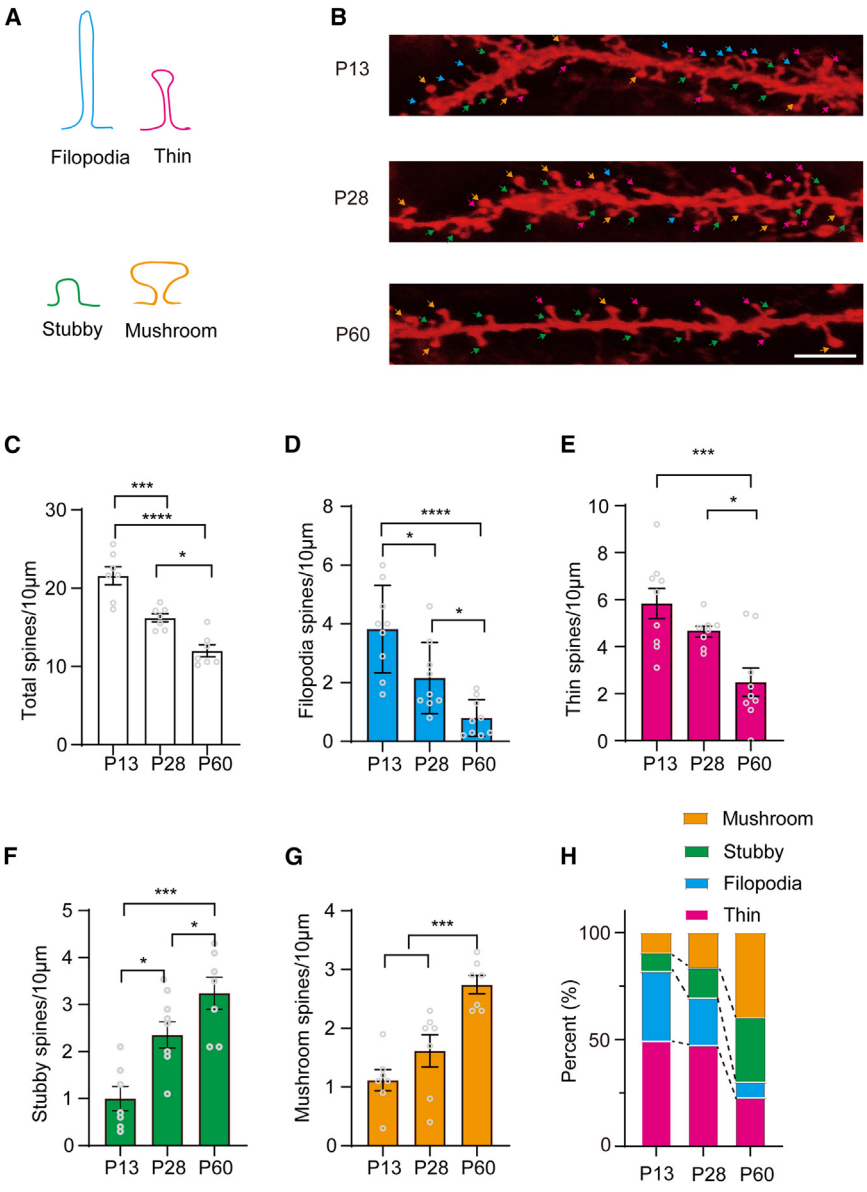

Figure 3. Spine morphological transitions in SC are developmentally regulated

(A) Schematic representation of four types of spine morphologies.

(B) Representative images of a three-dimensional stack of SC dendrites at different ages (P13, P28, P60). Colored arrowheads point to protrusions that are analyzed further in the below panels. Scale bars, 10 μm.

(C) Quantification of total number of spines per 10-μm dendrites at different ages (7 mice per group). Spine densities were calculated by quantifying the number of spines per 10-μm dendritic length. The averaged spine density of each mouse was counted by the mean value of five sections. Open circles represent each animal.

(D) Quantification of the number of filopodial-like spine densities at different ages (9 mice per group).

(E) Quantification of the number of thin-type spine densities at different ages (9 mice per group).

(F) Quantification of the number of stubby-type spine densities at different ages (7 mice per group).

(G) Quantification of the number of mushroom-type spine densities at different ages (7 mice per group).

(H) The mean percentage of the four types of spines varies with age (7 mice per age).

Data are presented as mean ± SEM. One-way ANOVA with Tukey's post hoc test for (C)–(G). *p < 0.05, **p < 0.01, ***p < 0.001, and ****p < 0.0001.

closure of the contralateral eye was performed at P13, P28, and P60. 4 days after MD, we examined the spine morphology in SC brain slices and found the total spine density was significantly reduced compared to non-deprived control mice only in the age group of P28 but not in P13 or P60 (Figures S5A–S5C). The proportions of filopodia, stubby, thin, and mushroom spines were not significantly altered by MD in any age group (Figure S5D). Taken together, these results reveal the impact of MD on the pruning of the SC spines during the critical period of development, indicating that SC spine morphology could reflect its OD plasticity.

SC OD plasticity was not due to corticofugal projection

The SC's visual response is determined by multiple sources of synaptic inputs, including the convergent inputs from bottom-up retinofugal projection and retinotopically organized top-down corticofugal projection from the V1.[41–48] Previous studies demonstrated that inactivation of the V1 reduced looming-evoked responses in many superficial SC neurons of awake, but not anesthetized, mice.[49] The corticofugal projection from layer 5 of the mouse V1 to the SC was shown to drive the light-induced arrest behavior.[50] Consistent with previous studies,[48,51] we injected cholera toxin subunit B with Alexa Fluor 594 conjugate (CTB594) in the SC and found retrogradely labeled neurons in the V1 (Figures 4A and 4B). The scale and timing of the OD shift in the SC is similar to the V1; thus, it is reasonable to ask if the SC OD plasticity we observed could be directly inherited from the V1. To test this, we pharmacologically inactivated V1 ipsilateral to the recorded SC by topical application of the $GABA_A$ receptor agonist muscimol (5 mM, Bio-Techne) to the brain surface, as described previously.[13] We recorded directly from deep layers of V1 (>500 μm) and found that muscimol almost completely abolished the spiking activities within 4–6 h (Figure 4C). However, the CBIs of SC binocular cells from MD mice were not affected by muscimol administration (0.50 ± 0.02; Figures 4D, S6A, and S6B). It is possible that the corticofugal projection affected the SC OD shift during the MD period, which cannot be tested with acute

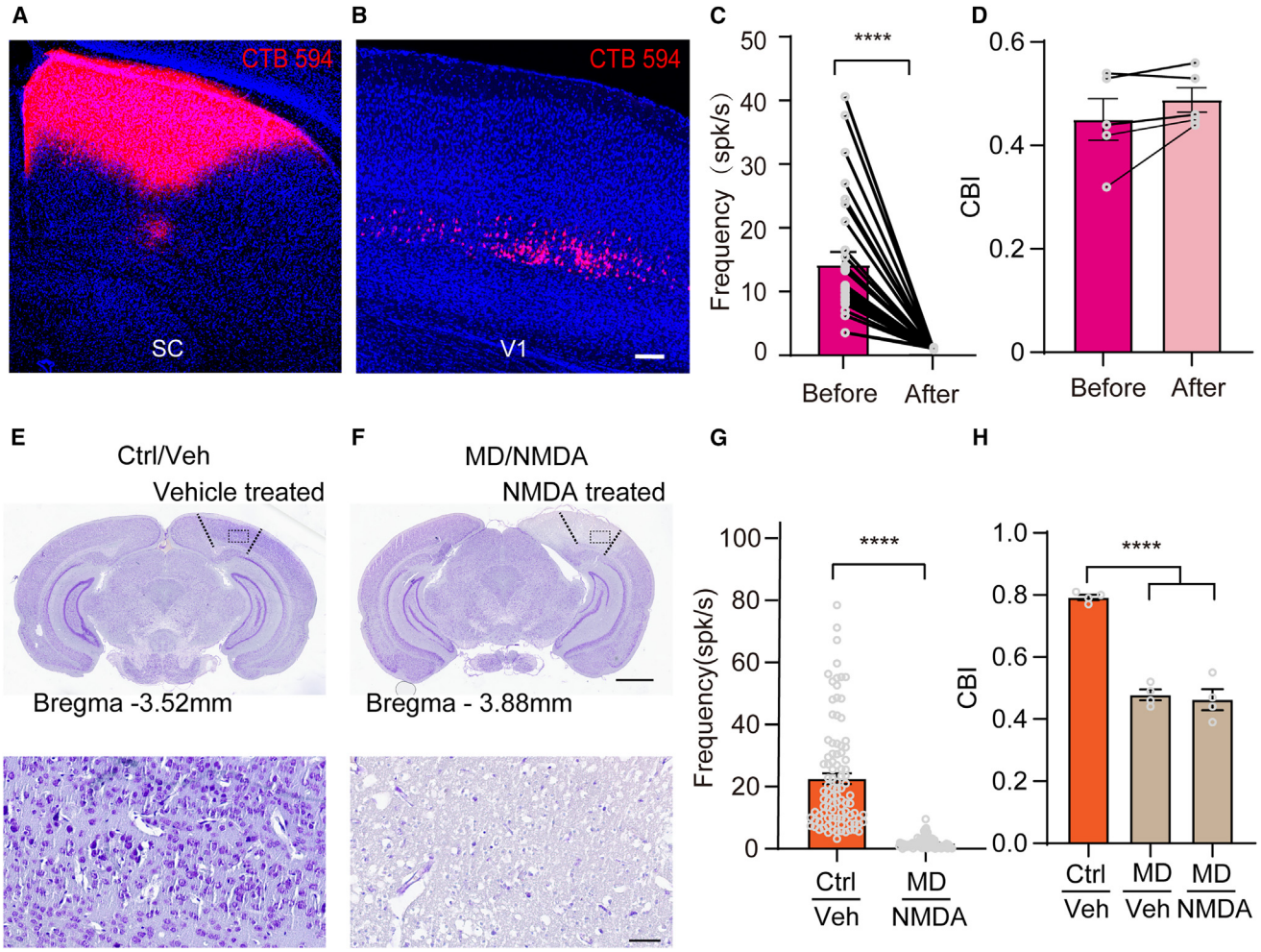

Figure 4. SC OD plasticity is not due to corticofugal projection

(A and B) Representative fluorescence images of CTB594 injection site in SC (A) and retrograde-labeled neurons in V1 (B), with DAPI staining cells. Scale bar, 100 μm.

(C) Summary plot of spike firing rate before and after muscimol administration (18 cells from 6 mice). Muscimol administration was able to silence all the recorded neurons in all directions.

(D) Mean CBIs for the SC of 4-day MD P28 mice before and after muscimol administration (5 mice). Open circles represent individual CBIs for each animal.

(E and F) Nissl-stained tissue section for vehicle (E) and NMDA (F) administration groups. Scale bar, 1,000 μm. The bottom images show enlarged views of the rectangle region in the top images. Scale bar, 50 μm.

(G) Summary plot of spike firing rate between vehicle (Ctrl, 266 cells from 6 mice) and NMDA (MD, 203 cells from 5 mice) administration groups in V1.

(H) The mean CBIs for SC are from vehicle (Ctrl, 207 cells from 4 mice), vehicle (MD, 127 cells from 4 mice), and NMDA (MD, 192 cells from 4 mice) administration groups.

Data are presented as mean ± SEM. Paired t test for (C), Mann-Whitney U test for (D), unpaired t test for (G), and one-way ANOVA with Tukey's post hoc test for (H). ****$p < 0.0001$.

muscimol silencing. To further test this, we conducted excitotoxic lesions in the V1 with NMDA injection[52,53] at P20 and MD starting at P28 and performed recordings at P32. NMDA lesion induced significant neuronal loss in the V1 (Figures 4E and 4F), and the neuronal firing was significantly reduced to near baseline (0.73 ± 0.08 spikes/s; Figure 4G). Our results revealed that a significant shift toward the ipsilateral (open) eye still occurred after NMDA inhibition of the V1 (0.46 ± 0.03; Figures 4H and S6C–S6E). Taken together, these results of acute V1 inactivation and prolonged V1 lesions suggested that the SC OD shifts were neither directly inherited nor indirectly affected by the V1. These results indicated that although the V1 is capable of providing top-down modulation of visual processing and is likely engaged in some visually guided behaviors, it may not be a major source of OD shifts in the SC.

Another major visual input source to the SC is the retina. The retinofugal input is important for the development and feature selectivity in the SC,[54,55] and it has been shown that retinal input can remodel after visual deprivation in mouse dLGN.[56,57] Thus, to answer if retinal input to the SC also undergoes remodeling

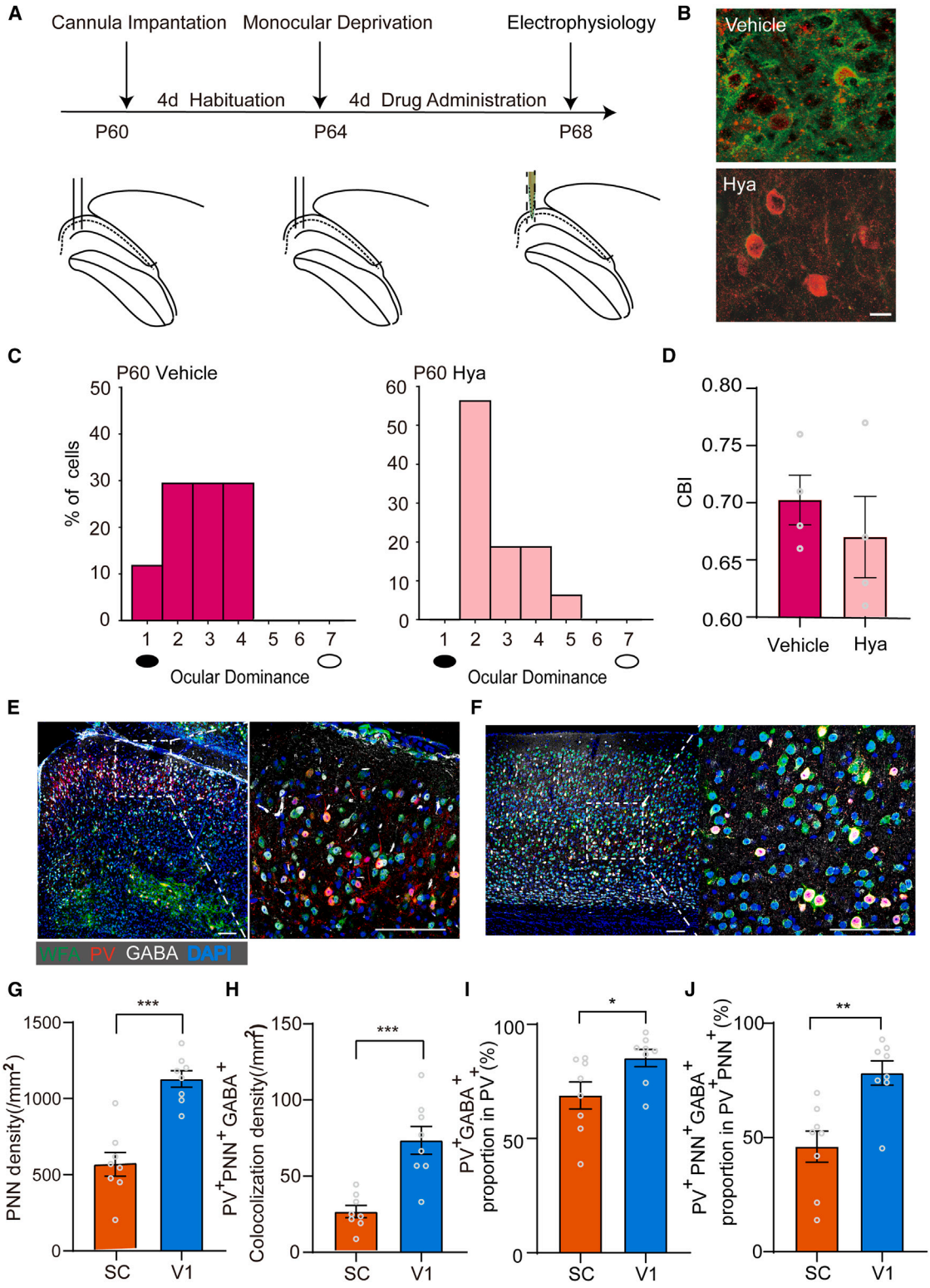

Figure 5. Hyaluronidase treatment does not reinstate functional plasticity in adult SC

(A) Schematic of the experimental procedure.

(B) The representative image of vehicle and hyaluronidase administration in SC. Scale bars, 20 μm.

(C) Distribution of OD scores for the SC of vehicle (346 cells from four mice) and hyaluronidase-treated (412 cells from four mice) groups.

(legend continued on next page)

after MD during the SC critical period, we injected two CTB dyes into mouse two eyes, respectively, with different fluorescent colors, together with 4-day MD starting at P16, P22, P30, and P60, and then imaged the SC slices to measure the fluorescent intensity, which represents the density of retinal axon terminals. Interestingly, we found that for the MD mice, the density of the contralateral retinal input was significantly reduced compared to control animals only in the age groups of P22 and P30 but not in the age groups of P16 and P60 (Figures S6F and S6G). This result suggests the retinofugal input to the SC indeed remodeled after MD during the critical period, indicating that retinal input remodeling could contribute to SC OD plasticity.

Hyaluronidase treatment could not reinstate OD plasticity in adult SC

The expression profile of perineuronal nets (PNNs) has been widely studied in many areas of the central nervous system of various animal species.[58–60] PNNs are unique extracellular matrix structures that wrap around many mature neurons in the brain, especially GABAergic neurons expressing the calcium-binding protein parvalbumin (PV), and restrict experience-dependent cortical plasticity.[61,62] To examine the impact of the degradation of PNNs on the reactivation of OD plasticity in the adult SC, we delivered hyaluronidase (Hya) into the mouse brain (Figure 5A), which was shown to degrade core components of the PNNs to promote V1 plasticity (Figure 5B) without inducing significant proliferation of astrocytes and microglia.[63] Interestingly, Hya treatment was not able to reinstate SC OD plasticity, as revealed by no significant difference in OD distribution and CBI value compared to vehicle-treated adult mice with 4-day MD (0.67 ± 0.05; Figures 5C and 5D).

The different regulation of adult OD plasticity in the V1 and SC via PNN degradation has several possible interpretations. First, the SC may not express as many PNNs as the V1; second, PNNs may regulate different neuron types in the V1 and SC, which have distinct roles in the regulation of OD plasticity. To ask how PNNs are expressed during the postnatal development of mouse SC and whether adult PNNs exert powerful inhibitory control of the SC, we applied WFA (wisteria floribunda agglutinin), a frequently used lectin that directly binds to N-acetylgalactosamine of polysaccharide glycosaminoglycan (GAG) chains of chondroitin sulfate proteoglycans (CSPGs), to characterize the distribution pattern of PNNs. Fluorescein isothiocyanate (FITC)-WFA revealed the differential distribution of PNNs in the SC and V1. In the V1, the middle layer possessed the highest relative PNN density, while the upper and deep layers had lower but still substantial densities (Figure 5F), whereas in the SC, WFA expression is concentrated in a discrete sublamina of the superficial layer with weaker or even no WFA in the deeper layer (Figure 5E). Significant differences were observed in the density of PNN^+ cells in the SC (560.50 ± 77.78/mm^2) versus the V1 (1,129.10 ± 54.48/mm^2; Figure 5G). This suggests that our first interpretation is valid. Next, to examine the PNN effects on specific cell types, we triple labeled PNN, PV, and GABA and found significant differences in the density of PNN^+ PV^+GABA^+ colocalized cells between the V1 (73.54 ± 9.18/mm^2) and the SC (25.42 ± 4.01/mm^2; Figure 5H). Furthermore, we observed a higher proportion of PV^+GABA^+ colocalized neurons in PV^+ neurons in the adult V1 (85.25% ± 3.79%), whereas in the SC, the colocalization rate was significantly lower (68.87% ± 5.90%; Figure 5I), consistent with previous studies showing that PV cells in the SC could be both excitatory and inhibitory.[64,65] A similar tendency was also observed in the percentage of PNN^+ PV^+GABA^+ cells in PNN^+ PV^+ cells (SC: 46.05% ± 6.84%, V1: 78.29% ± 3.34%; Figure 5J), suggesting that unlike the V1, in the SC, a large portion of the PNN and PV colocalized cells are excitatory neurons. This suggests that our second interpretation is also valid.

Since PNN^+ cells did not regulate SC OD plasticity, we wanted to know what other cell types could be regulators for it. It is known that the NRG1-ErbB4 signaling pathway is essential for the functions of GABAergic neurons in both the hippocampus and neocortex.[66] The mice lacking the NRG1 or ErbB4 gene show significant deficits in migration, axon and dendrite development, and synaptogenesis of interneurons. Recent studies found that NRG1-ErbB4 signaling can regulate the neuroplasticity of PV^+ inhibitory neurons in the V1.[67,68] Meanwhile, the expression of NRG1 is high in the critical period of the V1 but is reduced in adulthood, suggesting that it may be a key molecule involved in the regulation of OD plasticity. To compare the participation of PV^+ and $NRG1^+$ cells in the OD plasticity of the V1 and SC, we did double labeling of PV and NRG1 and measured their density and colocalization after MD in juvenile mice (Figures S7A–S7D). We found that MD induced a significant decrease of PV^+ cell density in the V1, but not in the SC (Figures S7E and S7F), consistent with the above result that PV^+ cells in the SC may have multiple roles. Interestingly, after MD, the PV^+NRG1^+ cell density decreased in both the SC and V1, suggesting that they participated in OD plasticity (Figures S7G and S7H). Considering PV^+ cell density also decreased in the V1, this result indicates that the PV^+NRG1^+ double-labeled cells might play a more substantial role in the regulation of SC OD plasticity than they did in the V1.

SC OD plasticity was both NR2B- and NR2A dependent

In both the V1 and hippocampus,[69,70] a developmental change of expression of NR2A- and NR2B-containing NMDA receptors

(D) Mean CBIs of both groups are shown in (C). Open circles represent individual CBIs for each animal.
(E) Example image of the SC staining with FITC-wisteria floribunda agglutinin (WFA; green), Alexa 555 anti-parvalbumin antibody (PV; red), GABA antibody (GABA; white), and DAPI (blue) in P60 mice. The right image shows an enlarged view of the rectangle region.Scale bar, 100 μm.
(F) Example image of the binocular V1 staining with antibodies as in (E) in P60 mice. Scale bar, 100 μm.
(G) Quantification of the density of PNN^+ cells in SC and V1 (32 sections from 8 mice). The average cell density of each mouse was counted by the mean value of four sections.
(H) Quantification of the density of $PV^+PNN^+GABA^+$ in SC and V1 (32 sections from 8 mice).
(I) Quantification of the percentage of PV^+GABA^+ cells in PV^+ neurons in SC and V1 (32 sections from 8 mice).
(J) Quantification of the percentage $PV^+PNN^+GABA^+$ cells in PV^+PNN^+ neurons in SC and V1 (32 sections from 8 mice).
Data are presented as mean ± SEM. Mann-Whitney U test for (D) and (G)–(J). *$p < 0.05$, **$p < 0.01$, and ***$p < 0.001$.

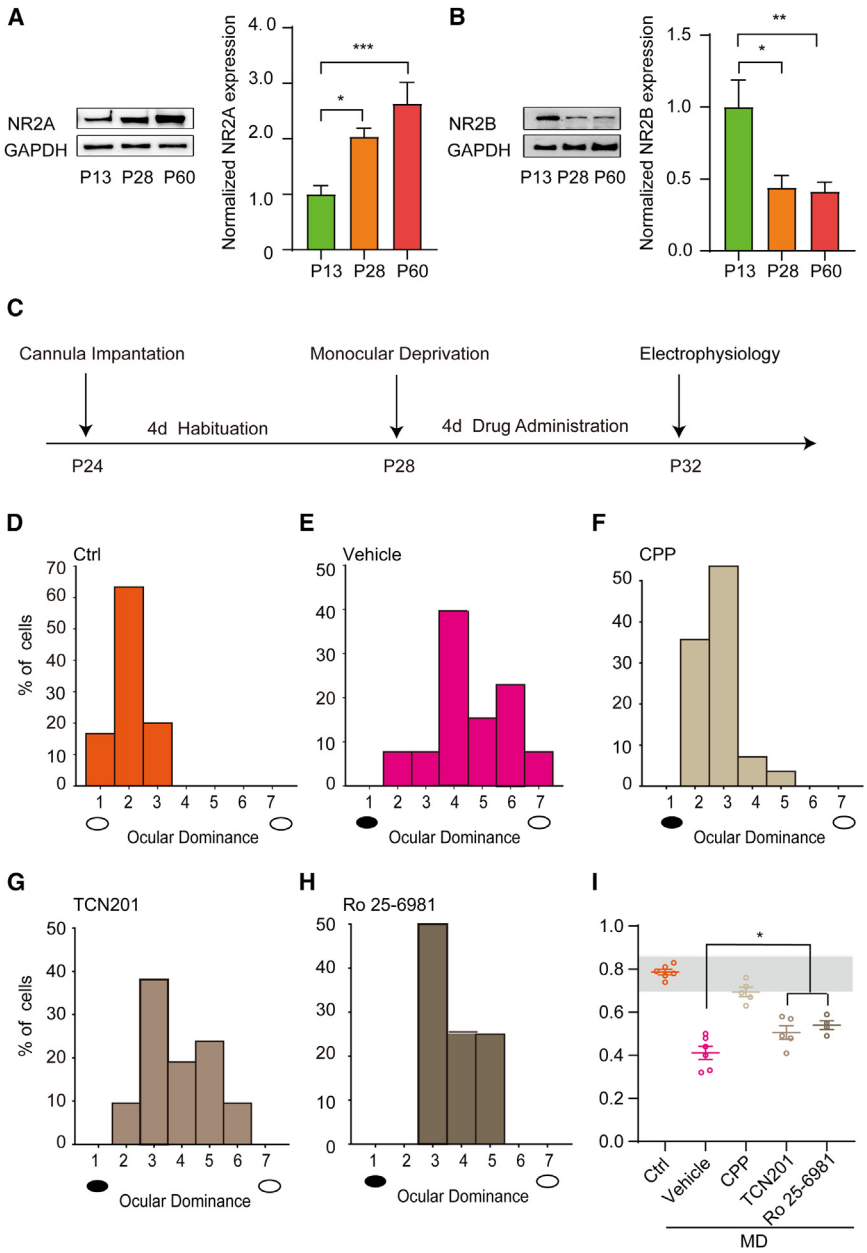

Figure 6. SC OD plasticity is both NR2A- and NR2B dependent

(A) Cropped images and quantifications of immunoblotting for NR2A protein expression in SC over development (10 mice per group). GAPDH was used as the internal standard.

(B) Cropped images and quantifications of immunoblotting for NR2B protein expression in SC over development (9 mice per group).

(C) Schematic of the experimental procedure.

(D–F) Distribution of OD scores for the SC of the Ctrl (D, 216 cells from 6 mice), vehicle (E, 271 cells from 6 mice), and NMDAR antagonist CPP (F, 192 cells from 5 mice) groups.

(G and H) Distribution of OD scores for the SC of local infusion of NR2A antagonists TCN 201 (G, 204 cells from 5 mice) and NR2B antagonist Ro 25-6981 (H, 127 cells from 4 mice) groups.

(I) A summary of the CBIs in each aforementioned group. Open circles represent individual CBIs for each animal.

Data are presented as mean ± SEM. One-way ANOVA with Tukey's post hoc test for (A), (B), and (I). *$p < 0.05$, **$p < 0.01$, and ***$p < 0.001$.

is thought to underlie the synaptic plasticity during early postnatal development.[71–75] Previous studies have linked NMDA receptor function to synaptic refinement after eye opening in the superficial layers of the SC *in vitro*.[76] Therefore, we asked whether the composition of NMDA receptors can regulate the OD plasticity of the developing SC *in vivo*. To find the developmental changes of NMDA receptor subunit composition, SC tissues were prepared at different postnatal ages (P13, P28, P60) and processed for western blot analysis. The result revealed that in the SC, the NR2A expression level increased approximately 2-fold from P13 to P28, which is the peak of the SC critical period plasticity, and became more prevalent in adult mice (P13: 1.00 ± 0.15, P28: 2.03 ± 0.16, P60: 2.63 ± 0.38; Figure 6A). In contrast, the more prevalent subunit at the onset of the critical period, NR2B, decreased progressively from P13 to P28 and was maintained at a low level throughout adulthood (P13: 1.00 ± 0.19, P28: 0.44 ± 0.08, P60: 0.41 ± 0.06; Figure 6B), similar to the results reported in the V1.[72,75]

Daily injection of the NMDA receptor antagonist CPP ((RS)-3-(2-Carboxypiperazin-4-yl)-propyl-1-phosphonic acid) into the SC prevented OD shift at P28 (0.70 ± 0.02; Figures 6D, 6F, and 6I). To distinguish the contributions of the NR2A and NR2B subunits on SC OD plasticity, we used an osmotic pump to locally infuse the NR2A antagonist TCN 201, the NR2B antagonist Ro 25-6981, or vehicle (artificial cerebrospinal fluid [ACSF] solution) daily into the SC of P28 mice throughout the 4-day MD (Figure 6C). Strikingly, the OD shift was partially blocked by NR2B and NR2A antagonists alone, resulting in a modest reduction of CBI, which was the intermediate between the control and vehicle groups (TCN 201: 0.51 ± 0.03, Ro 25-6981: 0.54 ± 0.02; Figures 6E and 6G–6I). Collectively, these findings revealed that NR2A- and NR2B-containing NMDA receptors together played a substantial role in OD plasticity of the developing SC.

Blocking the NMDA receptor in SC partially prevented the predatory impairments after the MD

It was reported that successful predatory hunting in mice requires both SC[77] and binocular vision,[78,79] raising the possibility that binocular-related OD plasticity within the SC plays a critical

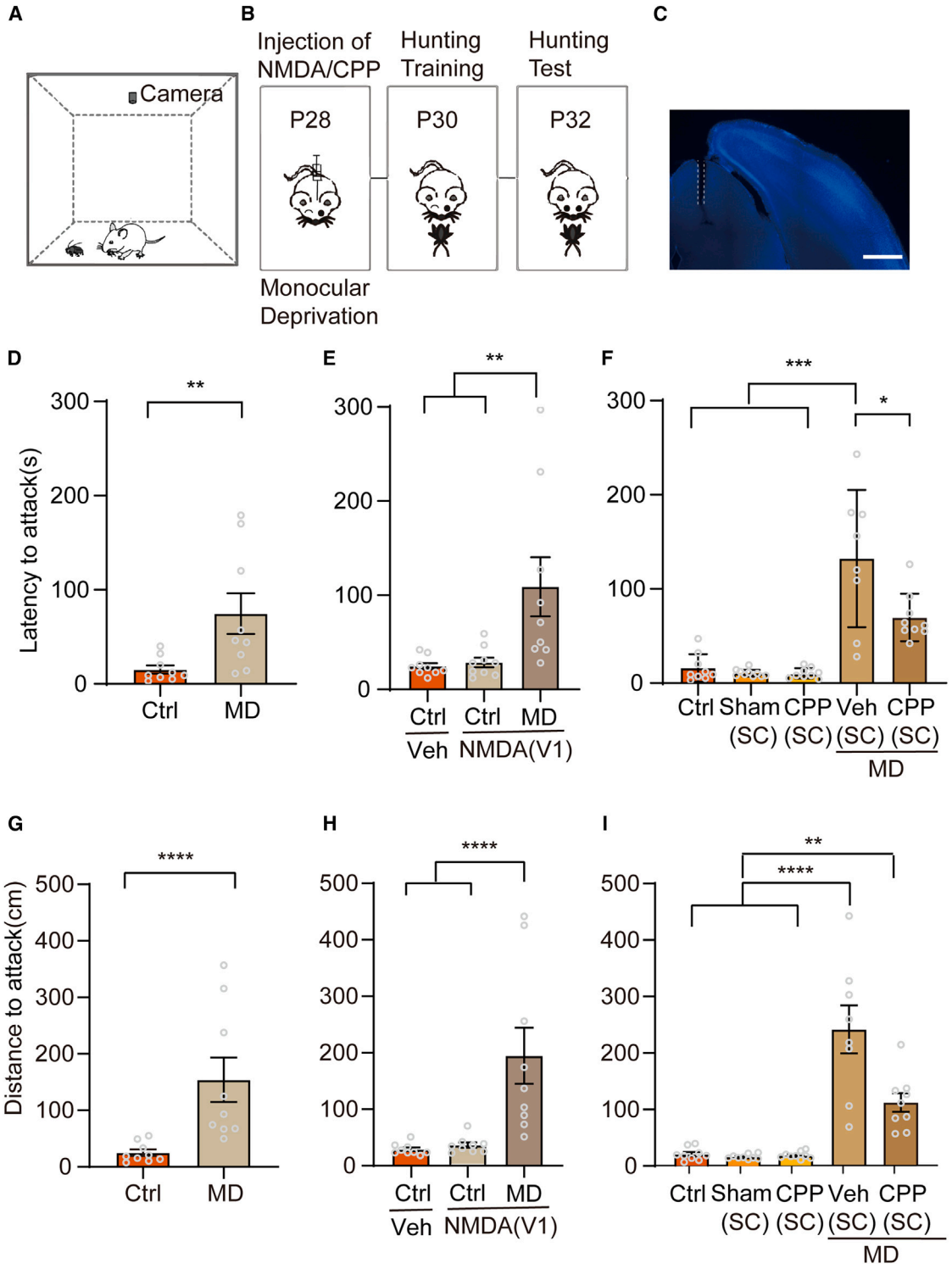

Figure 7. Blocking NMDA receptor in SC partially restores impaired predatory hunting efficiency after MD

(A) Schematic of the behavioral paradigm to monitor predatory hunting in mice.

(B) Schematic of the procedure for testing hunting efficiency after MD and drug infusion.

(C) Example micrographs showing the cannula track demarcated with dashed white lines. Scale bar, 1,000 μm.

(D) Quantitative analyses of latency to attack for Ctrl and MD mice (9 mice for each group). Each circle indicates an individual mouse.

(legend continued on next page)

role in this behavior. To explore whether the OD plasticity in mouse SC can influence hunting efficiency, we set up a paradigm to quantitatively analyze predatory hunting in mice. The hunting test began with the introduction of a cricket (prey) to a mouse (predator) in an arena, and the mouse behavior was recorded using an overhead camera (Figure 7A).

We performed MD from P28 until P32 to induce OD shift (Figure 7B). MD mice took a longer time (Ctrl: 16.00 ± 4.89 s, MD: 74.33 ± 21.77 s; Figure 7D) to initiate the attack compared to Ctrls, consistent with previous results.[78,80] To confirm whether hunting efficiency was influenced by the OD shift in the SC or V1, we conducted pharmacological bilateral lesions of either V1 or SC with NMDA at P28.[52] We found that NMDA lesion in the bilateral V1 did not affect impaired hunting efficiency after MD, as the animals still showed a higher latency to attack (97.89 ± 27.80 s; Figure 7E). However, when NMDA was bilaterally injected into lesioned SC, almost none of the mice (2/10) could successfully capture the crickets after behavioral training, confirming the critical role of the SC in predatory hunting.[77,81] Furthermore, to inhibit the OD shift in the SC after MD, we injected CPP into the SC daily during the MD period (Figure 7C) and found that the latency for MD mice to attack crickets significantly reduced (69.67 ± 8.44 s; Figure 7F), suggesting that the impairment after MD was partially prevented by CPP injection in the SC. It should be noted that the CPP administration did not change the neuronal firing rates in the SC (Figure S8).

The reduction of attack latency in MD mice could be explained by impairments in either the precise localization of the prey (visual cue) or the motivation to hunt the prey. To differentiate these two possibilities, we further quantify the distance the mice traveled from introduction to the first bite/contact (Figure S9). We found that MD significantly increased the distance to attack (Ctrl: 23.06 ± 5.73 cm, MD: 154.10 ± 39.31 cm; Figure 7G), but NMDA lesion in the bilateral V1 did not change this trend (194.70 ± 49.51 cm; Figure 7H), while CPP treatment in the SC significantly reduced the distance to attack for MD mice (110.40 ± 16.27 cm; Figure 7I). In addition, both attack duration and attack frequency are not affected by MD, NMDA, or CPP administration (Figure S10). These results suggest that the effect of MD was not due to an impairment in the hunting motivation.

To further confirm that the effects of MD were due to the impairment in the precise localization of the visual cue, but not of other sensory inputs, we repeated the above behavioral test in a completely dark environment, with whiskers removed, or a combination of the two. We found that reduced hunting efficiency after MD only existed in a normal light environment and was absent without visual cues (Figure S11), confirming that the MD-induced SC-related predatory efficiency reduction was mediated through visual inputs.[82] In addition, since the training period in the above behavioral paradigm was coincidental with the MD period, the deficits could be due to insufficient training. To rule out this possibility, we performed another experiment in which the MD mice were trained with both eyes open after the MD period and found that significant increases in latency to attack still existed (Figure S12), suggesting they could not be due to the difference between monocular or binocular training processes. Taken together, MD severely impaired predatory hunting efficiency, and this deficit could be partially prevented by blocking the OD shift in the SC.

DISCUSSION

In addition to prevailing models of V1 OD plasticity, in the current study, we demonstrated that the changes in eye-specific responses after MD also occurred in the SC. Periods of MD as short as 4 days produced a robust shift in the responsiveness of SC binocular neurons toward the non-deprived eye, and these effects were restricted to a time window similar to the V1 critical period. OD shift in the SC could specifically reduce predatory hunting efficiency, with no effects on attack or consumption phases, and this deficit could be partially prevented by NMDA receptor blockade.

Prevalence of binocularity in mouse SC

Most previous studies in the rodent SC suggest minimal binocular interactions[30,83]; in contrast, our results found that a surprising proportion of the neurons in mouse SC exhibited binocular response, suggesting that binocular interactions in mouse SC are more prevalent than previously assumed, which is consistent with a recent publication.[31] The discrepancy with the previous literature could be due to the improvement of the data acquisition system, which promotes the signal exaction from the noise. Interestingly, a recent study demonstrated a more widespread binocular integration in mouse V1 than previously thought, probably due to the differences in the acquisition technique and the definition of the binocular integration used.[84] The same could also apply to our study. Recent works suggest robust differences in visual tuning in the awake state compared to the anesthetized state, including increased responsiveness,[49] spontaneous activity, and contrast sensitivity.[85] Thus, the neurons responding strongly to ipsilateral inputs may be more easily identified in a

(E) Quantitative analyses of latency to attack for Ctrl subjected to bilateral vehicle administration and Ctrl and MD mice with bilateral V1 lesions (9 mice for each group).
(F) Quantitative analyses of latency to attack for Ctrl, Ctrl mice subjected to sham surgery/CPP-only administration, and MD mice subjected to vehicle/CPP administration in SC (8–10 mice for each group).
(G) Quantitative analyses of distance to attack for Ctrl and MD mice (9 mice for each group).
(H) Quantitative analyses of distance to attack for Ctrl subjected to bilateral vehicle administration and Ctrl and MD mice with bilateral V1 lesion (9 mice for each group).
(I) Quantitative analyses of distance to attack for Ctrl, Ctrl mice subjected to sham surgery/CPP-only administration, and MD mice subjected to vehicle/CPP administration in SC (8–10 mice for each group).
Data are presented as mean ± SEM. Mann-Whitney U test for (D) and (G) and one-way ANOVA with Tukey's post hoc test for (E), (F), (H), and (I). *$p < 0.05$, **$p < 0.01$, ***$p < 0.001$, and ****$p < 0.0001$.

relatively sober state. Future studies leveraging eye-specific manipulations of activity remain to be conducted to resolve the underlying mechanism.

Similarities of the critical period for OD plasticity between SC and V1

Our data showed that 4-day MD was sufficient to induce an OD shift of SC binocular neurons toward the non-deprived eye in juveniles. Although 2-day deprivation in the V1 is quite effective, 4-day deprivation is required for a maximal effect.[5,86] 2-day deprivation in the SC is insufficient to induce a significant shift toward the non-deprived eye, suggesting that the SC might have a higher threshold to initiate OD shift. Our data support the conclusion that the extent of SC OD plasticity varies significantly with age, similar to the V1.[87] Robust OD shift in response to prolonged MD has been revealed in the V1 of adult mice,[34] rats,[88] cats,[89,90] and primates.[91] A delayed potentiation of the response to stimulation of the non-deprived eye can account for the OD shift in adults, which is related to homeostatic plasticity.[35] Furthermore, the OD shift in adult SC could be induced with 8-day MD, indicating that a similar homeostatic plasticity could exist in the adult SC binocular neurons.

The changes in spine morphology probably have a crucial role in the development and plasticity of the nervous system.[36] Despite a long history of research, the relation between morphological changes in spines and OD plasticity is still not well understood. In line with a previous study,[92] we found that filopodia-like dendritic protrusions are abundant in juvenile animals but virtually absent in adults. In juvenile mice, within the critical period for V1 development, most of the spines remain stable over a 1-month interval. In contrast, in adult mice, a higher ratio of spines remains stable.[92] Classic studies have demonstrated heightened functional and anatomical plasticity within critical periods, during which the developing nervous system can be rapidly and permanently modified by experience.[89,93] However, one unexplainable question was why the maximal decline effects of 4-day MD started at P28 but lost its trend at P32. What could give rise to the structural basis underlying this transition from a plastic state to a more stable state within 4 days remains unknown. One plausible explanation is that sensory deprivation did not change the density, length, or shape of spines but markedly reduced protrusive motility[94]; thus, it is conceivable that OD plasticity may be more closely correlated with spine motility,[95] which is hard to image in the SC with *in vivo* two-photon microscopy unless with an implanted gradient-index lens or with the cortex removed,[96] or even with "cortexless" mice.[52] Also, morphological changes in spines might occur as a consequence of experience but are not the cause of plasticity.[36]

The specific composition of NMDA receptor subunits is thought to underlie the OD plasticity of the cortex.[97] NR2A and NR2B are two predominant regulatory subunits of NMDA receptors in the V1. A developmental change in the expression level of NR2A/B subunits occurs concurrently with the decline of visual plasticity,[74,75] which is reversed after visual deprivation.[75,98] Here, we showed a similar developmental change of NR2A/B subunit expression during SC maturation, which is consistent with previous studies in the V1 and other brain areas.[72,73,75] Blocking NMDA receptors with CPP prevented the MD-induced OD shift in the SC. NR2A-containing receptors are required for the induction of long-term potentiation (LTP), whereas NR2B receptors are required for the induction of long-term depression (LTD).[98,99] Both were shown to play a role in our study, suggesting that SC OD plasticity involves a Hebbian synaptic plasticity mechanism.

Differences in the critical period for OD plasticity between SC and V1

Most previous studies have investigated the impact of cortical input on the SC's feature selectivity in different species, including mice,[49,50,96,100] cats,[101–103] and monkeys.[104] The effect of cortical input on the superficial SC's responsiveness has been reported to be facilitatory,[105] suppressive,[101] or insignificant.[96] Response selectivity of SC cells has been reported to be either dependent[103] or independent[96] of cortical input. Since the substantial contribution of corticotectal input on the SC could be completely masked by anesthesia,[49] it would be interesting to ask whether the SC OD shift in awake mice could be influenced by the corticotectal input. In this study, we found that acute inhibition or sustained lesion of V1 had only negligible influence on eye-specific changes of SC responses after MD. Unlike response magnitude, our results indicated that cortical input does not participate in the OD plasticity of SC cells in anesthetized mice. Similarly, the speed tuning, response temporal dynamics, and selectivity in the SC were not affected by removing cortical input, albeit with different visual stimuli.[49] Since cortical input largely acts as a gain control to the SC,[49] it is possible that silencing the V1 in the awake state would reduce the response magnitude of contralateral and ipsilateral inputs proportionally and concurrently, thus not affecting OD shift.

Similar to previous data,[106–108] our immunohistological results showed that PV expression was distributed predominantly in a sublamina of the superficial SC. OD plasticity could be rescued in adult V1 by Hya via degrading core components of the PNNs.[62,63,75,109] CSPG's inhibitory effect on axonal sprouting suggests that degradation of PNNs could remove non-permissive substrates for experience-dependent rearrangement of synaptic connections.[61,109,110] Interestingly, we found that removing PNNs with Hya administration was ineffective in restoring OD plasticity in adult SC. Our data indicate that this inconsistency could be attributed to the lower expression of PNN^+ neurons, and PNNs in the SC may not affect as many PV^+ inhibitory neurons as the V1. This indicates that the PV-mediated modulation of OD plasticity in the V1 might not play an important role in the SC. Our PV^+NRG1^+ staining data also supported this interpretation.

Relationship between predatory behavior and SC plasticity

Accumulating literature has evidenced that projection-defined SC-related circuits participate in predator avoidance,[111] prey-derived sensory cues detection, and prey-capture behavior initiation.[112] Binocular vision, which combines information from the visual field shared by both eyes, is thought to be essential for predation.[78,82] Although it is known that the superficial layers of the SC primarily receive visual inputs from the retina and V1,[113] whether SC OD shift guides predation and influences hunting success remains unknown. The hunting behavior

typically contains stereotyped motor programs, such as prey search, pursuit, attack, and consumption.[114] Prey detection might originate in the retina, as some RGCs are visually sensitive to simple stimuli such as approaching visual stimuli or light flashes.[115,116] Binocular vision can break a prey's camouflage, estimate the distance between predator and prey more accurately than monocular vision, and improve sensitivity in dim light and low contrast. Our results are consistent with previous studies that visual deprivation significantly increased the latency (and distance) to attack but not the attacking frequency or duration.[78,80] Furthermore, we showed that the impairment was directly contributed by SC neurons rather than from the V1. Our results are at odds with previous studies[112] in that simultaneous bimodal sensory deprivation did not exert an additive effect on reducing hunting efficiency. One possible explanation is that apart from vibrissal somatosensory and visual cues, other sensory modalities, such as auditory cues[117,118] and olfactory senses,[118–122] could also be involved for predators to distinguish prey from the background. The other possible explanation is that besides SC-related circuits, other brain regions also directly or indirectly interfere with hunting behavior, such as the lateral hypothalamus,[123,124] periaqueductal gray,[114] and dorsal anterior cingulate.[125–127] It would be interesting to directly record SC neuronal activity during prey behavior to see if different groups of SC neurons encode distinct hunting phases.

Regardless of the precise mechanisms that remain to be examined, our results showed that the eye-specific responses of SC binocular neurons were not rigid but underwent pronounced functional OD plasticity. While it still needs to be established to what degree data obtained in mouse SC could be generalized to humans, it seems that the current finding of OD plasticity in mouse SC should make us reevaluate the purely cortical interpretations of amblyopia, and the previous treatment for amblyopia may have neglected an important affected central locus.

Limitations of the study

There are several limitations of the study. First of all, the absolute changes in the SC responses to deprived-eye and non-deprived-eye stimulation remain unexplored, so we cannot ascertain whether there exist two temporally distinct processes causing the SC OD shift after MD, as in the V1. This could be examined with a chronic recording method to document the kinetics of OD shift in mouse SC. Moreover, owing to technical difficulties, it remains challenging to assess whether remodeling of RGC axons underlies OD plasticity at the synaptic level, which would require *in vivo* functional and structural approaches to help address this. Last but not the least, we still do not know the exact role that NRG1 plays in the regulation of SC OD plasticity. A further in-depth investigation of NRG1's role requires additional studies of the complete signaling pathway downstream of NRG1, which could probably lead to a change of the balance between excitation and inhibition (E-I balance) or NMDA receptor functions.

STAR★METHODS

Detailed methods are provided in the online version of this paper and include the following:

SUPPLEMENTAL INFORMATION

Supplemental information can be found online at https://doi.org/10.1016/j.celrep.2023.113667.

ACKNOWLEDGMENTS

We would like to acknowledge Dr. Jianhua Cang (UVa), Dr. Jiayi Zhang (Fudan University), Dr. Yongmei Zhong (Fudan University), Dr. Shijun Weng (Fudan University), and Dr. Xiaoming Zhou (ECNU) for helpful discussions and insightful advice. We would also like to thank Dr. Meng Pan (Tianjin Medical University), Ms. Yijing Yan, and Mr. Xinyu Li (Tianjin Medical University) for their help in collecting and analyzing the data. This work is supported by the National Natural Science Foundation of China (31872764 and 82171090 to Y.G. and 81770956 and 81371049 to X.S.), the Shanghai Science and Technology Committee Rising-Star Program (19QA1401600 to Y.G.), the Shanghai Municipal Science and Technology Major Project (no. 2018SHZDZX01), ZJLab, the Shanghai Center for Brain Science and Brain-Inspired Technology, the Lingang Laboratory (LG-QS-202203-12), the Project of Tianjin 131 Innovative Talent Team (201936 to X.S. and Y.G.), the Science Fund for Distinguished Young Scholars of Tianjin (17JCJQJC46000 to X.S.), the Science and Technology Planning Project of Tianjin (no. 21JCYBJC00780 to X.S.), the Jinmen Medical Talent Project of Tianjin, the Science and Technology Fund for Health of Tianjin (TJWJ2023ZD008 to X.S.), and the Tianjin Key Medical Discipline (Specialty) Construction Project (no. TJYXZDXK-016A).

AUTHOR CONTRIBUTIONS

Conceptualization, G.H., X.S., and Y.G.; methodology, G.H., A.C., J.W., J.Y., Q.L., M.H., and M.D.; formal analysis, G.H., A.C., C.F., J.Y., and X.W.; investigation, G.H., A.C., and J.Y.; writing – original draft, G.H.; writing – review & editing, X.S. and Y.G.; supervision, X.S. and Y.G.

DECLARATION OF INTERESTS

The authors declare no competing interests.

Received: May 11, 2023
Revised: September 29, 2023
Accepted: December 25, 2023

REFERENCES

1. Hensch, T.K. (2005). Critical period plasticity in local cortical circuits. Nat. Rev. Neurosci. *6*, 877–888.
2. Hensch, T.K. (2004). Critical period regulation. Annu. Rev. Neurosci. *27*, 549–579.
3. Hubel, D.H., and Wiesel, T.N. (1970). The period of susceptibility to the physiological effects of unilateral eye closure in kittens. J. Physiol. *206*, 419–436.
4. LeVay, S., Wiesel, T.N., and Hubel, D.H. (1980). The development of ocular dominance columns in normal and visually deprived monkeys. J. Comp. Neurol. *191*, 1–51.
5. Gordon, J.A., and Stryker, M.P. (1996). Experience-dependent plasticity of binocular responses in the primary visual cortex of the mouse. J. Neurosci. *16*, 3274–3286.
6. Lehmann, K., and Löwel, S. (2008). Age-dependent ocular dominance plasticity in adult mice. PLoS One *3*, e3120.
7. Gilbert, C.D., and Wiesel, T.N. (1992). Receptive field dynamics in adult primary visual cortex. Nature *356*, 150–152.
8. Hooks, B.M., and Chen, C. (2020). Circuitry Underlying Experience-Dependent Plasticity in the Mouse Visual System. Neuron *106*, 21–36.
9. Derrington, A.M., and Hawken, M.J. (1981). Spatial and temporal properties of cat geniculate neurones after prolonged deprivation. J. Physiol. *314*, 107–120.
10. Blakemore, C., and Vital-Durand, F. (1986). Effects of visual deprivation on the development of the monkey's lateral geniculate nucleus. J. Physiol. *380*, 493–511.
11. Levitt, J.B., Schumer, R.A., Sherman, S.M., Spear, P.D., and Movshon, J.A. (2001). Visual response properties of neurons in the LGN of normally reared and visually deprived macaque monkeys. J. Neurophysiol. *85*, 2111–2129.
12. Wiesel, T.N., and Hubel, D.H. (1963). Effects of visual deprivation on morphology and physiology of cells in the cat's lateral geniculate body. J. Neurophysiol. *26*, 978–993.
13. Jaepel, J., Hübener, M., Bonhoeffer, T., and Rose, T. (2017). Lateral geniculate neurons projecting to primary visual cortex show ocular dominance plasticity in adult mice. Nat. Neurosci. *20*, 1708–1714.
14. Sommeijer, J.P., Ahmadlou, M., Saiepour, M.H., Seignette, K., Min, R., Heimel, J.A., and Levelt, C.N. (2017). Thalamic inhibition regulates critical-period plasticity in visual cortex and thalamus. Nat. Neurosci. *20*, 1715–1721.
15. Rose, T., and Bonhoeffer, T. (2018). Experience-dependent plasticity in the lateral geniculate nucleus. Curr. Opin. Neurobiol. *53*, 22–28.
16. Li, N., and Gu, Y. (2020). The Visual Pathway for Binocular Integration. Neurosci. Bull. *36*, 1089–1091.
17. Cang, J., Savier, E., Barchini, J., and Liu, X. (2018). Visual Function, Organization, and Development of the Mouse Superior Colliculus. Annu. Rev. Vis. Sci. *4*, 239–262.
18. Dräger, U.C., and Hubel, D.H. (1975). Responses to visual stimulation and relationship between visual, auditory, and somatosensory inputs in mouse superior colliculus. J. Neurophysiol. *38*, 690–713.
19. Cooper, B., and McPeek, R.M. (2021). Role of the Superior Colliculus in Guiding Movements Not Made by the Eyes. Annu. Rev. Vis. Sci. *7*, 279–300.
20. Gandhi, N.J., and Katnani, H.A. (2011). Motor functions of the superior colliculus. Annu. Rev. Neurosci. *34*, 205–231.
21. Liu, X., Huang, H., Snutch, T.P., Cao, P., Wang, L., and Wang, F. (2022). The Superior Colliculus: Cell Types, Connectivity, and Behavior. Neurosci. Bull. *38*, 1519–1540.
22. Yu, Q., Fu, H., Wang, G., Zhang, J., and Yan, B. (2021). Short-Term Visual Experience Leads to Potentiation of Spontaneous Activity in Mouse Superior Colliculus. Neurosci. Bull. *37*, 353–368.
23. Basso, M.A., Bickford, M.E., and Cang, J. (2021). Unraveling circuits of visual perception and cognition through the superior colliculus. Neuron *109*, 918–937.
24. Stein, B.E., Jiang, W., Wallace, M.T., and Stanford, T.R. (2001). Nonvisual influences on visual-information processing in the superior colliculus. Prog. Brain Res. *134*, 143–156.
25. Ellis, E.M., Gauvain, G., Sivyer, B., and Murphy, G.J. (2016). Shared and distinct retinal input to the mouse superior colliculus and dorsal lateral geniculate nucleus. J. Neurophysiol. *116*, 602–610.
26. Zhang, L.I., Tao, H.W., and Poo, M. (2000). Visual input induces long-term potentiation of developing retinotectal synapses. Nat. Neurosci. *3*, 708–715.
27. Tao, H.W., Zhang, L.I., Engert, F., and Poo, M. (2001). Emergence of input specificity of ltp during development of retinotectal connections in vivo. Neuron *31*, 569–580.
28. Lien, C.C., Mu, Y., Vargas-Caballero, M., and Poo, M.M. (2006). Visual stimuli-induced LTD of GABAergic synapses mediated by presynaptic NMDA receptors. Nat. Neurosci. *9*, 372–380.
29. van Rheede, J.J., Richards, B.A., and Akerman, C.J. (2015). Sensory-Evoked Spiking Behavior Emerges via an Experience-Dependent Plasticity Mechanism. Neuron *87*, 1050–1062.
30. Petros, T.J., Rebsam, A., and Mason, C.A. (2008). Retinal axon growth at the optic chiasm: to cross or not to cross. Annu. Rev. Neurosci. *31*, 295–315.
31. Russell, A.L., Dixon, K.G., and Triplett, J.W. (2022). Diverse modes of binocular interactions in the mouse superior colliculus. J. Neurophysiol. *127*, 913–927.
32. Hensch, T.K., Fagiolini, M., Mataga, N., Stryker, M.P., Baekkeskov, S., and Kash, S.F. (1998). Local GABA circuit control of experience-dependent plasticity in developing visual cortex. Science *282*, 1504–1508.
33. Ito, S., and Feldheim, D.A. (2018). The Mouse Superior Colliculus: An Emerging Model for Studying Circuit Formation and Function. Front. Neural Circuits *12*, 10.
34. Sato, M., and Stryker, M.P. (2008). Distinctive features of adult ocular dominance plasticity. J. Neurosci. *28*, 10278–10286.
35. Sawtell, N.B., Frenkel, M.Y., Philpot, B.D., Nakazawa, K., Tonegawa, S., and Bear, M.F. (2003). NMDA receptor-dependent ocular dominance plasticity in adult visual cortex. Neuron *38*, 977–985.
36. Yuste, R., and Bonhoeffer, T. (2001). Morphological changes in dendritic spines associated with long-term synaptic plasticity. Annu. Rev. Neurosci. *24*, 1071–1089.
37. Ebrahimi, S., and Okabe, S. (2014). Structural dynamics of dendritic spines: molecular composition, geometry and functional regulation. Biochim. Biophys. Acta *1838*, 2391–2398.
38. Hering, H., and Sheng, M. (2001). Dentritic spines : structure, dynamics and regulation. Nat. Rev. Neurosci. *2*, 880–888.
39. Chang, F.L., and Greenough, W.T. (1984). Transient and enduring morphological correlates of synaptic activity and efficacy change in the rat hippocampal slice. Brain Res. *309*, 35–46.
40. Peters, A., and Kaiserman-Abramof, I.R. (1970). The small pyramidal neuron of the rat cerebral cortex. The perikaryon, dendrites and spines. Am. J. Anat. *127*, 321–355.
41. Hallman, L.E., Schofield, B.R., and Lin, C.S. (1988). Dendritic morphology and axon collaterals of corticotectal, corticopontine, and callosal neurons in layer V of primary visual cortex of the hooded rat. J. Comp. Neurol. *272*, 149–160.

42. Hübener, M., Schwarz, C., and Bolz, J. (1990). Morphological types of projection neurons in layer 5 of cat visual cortex. J. Comp. Neurol. *301*, 655–674.

43. Wang, Q., and Burkhalter, A. (2013). Stream-related preferences of inputs to the superior colliculus from areas of dorsal and ventral streams of mouse visual cortex. J. Neurosci. *33*, 1696–1705.

44. Van Horn, S.C., Erişir, A., and Sherman, S.M. (2000). Relative distribution of synapses in the A-laminae of the lateral geniculate nucleus of the cat. J. Comp. Neurol. *416*, 509–520.

45. Gale, S.D., and Murphy, G.J. (2014). Distinct representation and distribution of visual information by specific cell types in mouse superficial superior colliculus. J. Neurosci. *34*, 13458–13471.

46. Harvey, A.R., and Worthington, D.R. (1990). The projection from different visual cortical areas to the rat superior colliculus. J. Comp. Neurol. *298*, 281–292.

47. Oh, S.W., Harris, J.A., Ng, L., Winslow, B., Cain, N., Mihalas, S., Wang, Q., Lau, C., Kuan, L., Henry, A.M., et al. (2014). A mesoscale connectome of the mouse brain. Nature *508*, 207–214.

48. Triplett, J.W., Owens, M.T., Yamada, J., Lemke, G., Cang, J., Stryker, M.P., and Feldheim, D.A. (2009). Retinal input instructs alignment of visual topographic maps. Cell *139*, 175–185.

49. Zhao, X., Liu, M., and Cang, J. (2014). Visual cortex modulates the magnitude but not the selectivity of looming-evoked responses in the superior colliculus of awake mice. Neuron *84*, 202–213.

50. Liang, F., Xiong, X.R., Zingg, B., Ji, X.Y., Zhang, L.I., and Tao, H.W. (2015). Sensory Cortical Control of a Visually Induced Arrest Behavior via Corticotectal Projections. Neuron *86*, 755–767.

51. Zingg, B., Chou, X.L., Zhang, Z.G., Mesik, L., Liang, F., Tao, H.W., and Zhang, L.I. (2017). AAV-Mediated Anterograde Transsynaptic Tagging: Mapping Corticocollicular Input-Defined Neural Pathways for Defense Behaviors. Neuron *93*, 33–47.

52. Diao, Y., Cui, L., Chen, Y., Burbridge, T.J., Han, W., Wirth, B., Sestan, N., Crair, M.C., and Zhang, J. (2018). Reciprocal Connections Between Cortex and Thalamus Contribute to Retinal Axon Targeting to Dorsal Lateral Geniculate Nucleus. Cereb. Cortex *28*, 1168–1182.

53. Kim, S.H., Won, S.J., Mao, X.O., Jin, K., and Greenberg, D.A. (2006). Molecular mechanisms of cannabinoid protection from neuronal excitotoxicity. Mol. Pharmacol. *69*, 691–696.

54. Shi, X., Barchini, J., Ledesma, H.A., Koren, D., Jin, Y., Liu, X., Wei, W., and Cang, J. (2017). Retinal origin of direction selectivity in the superior colliculus. Nat. Neurosci. *20*, 550–558.

55. Zhang, J., Ackman, J.B., Xu, H.P., and Crair, M.C. (2011). Visual map development depends on the temporal pattern of binocular activity in mice. Nat. Neurosci. *15*, 298–307.

56. Hooks, B.M., and Chen, C. (2006). Distinct roles for spontaneous and visual activity in remodeling of the retinogeniculate synapse. Neuron *52*, 281–291.

57. Hooks, B.M., and Chen, C. (2008). Vision triggers an experience-dependent sensitive period at the retinogeniculate synapse. J. Neurosci. *28*, 4807–4817.

58. Ye, Q., and Miao, Q.L. (2013). Experience-dependent development of perineuronal nets and chondroitin sulfate proteoglycan receptors in mouse visual cortex. Matrix Biol. *32*, 352–363.

59. Baker, K.D., Gray, A.R., and Richardson, R. (2017). The development of perineuronal nets around parvalbumin gabaergic neurons in the medial prefrontal cortex and basolateral amygdala of rats. Behav. Neurosci. *131*, 289–303.

60. Brückner, G., Grosche, J., Schmidt, S., Härtig, W., Margolis, R.U., Delpech, B., Seidenbecher, C.I., Czaniera, R., and Schachner, M. (2000). Postnatal development of perineuronal nets in wild-type mice and in a mutant deficient in tenascin-R. J. Comp. Neurol. *428*, 616–629.

61. Berardi, N., Pizzorusso, T., and Maffei, L. (2004). Extracellular matrix and visual cortical plasticity: freeing the synapse. Neuron *44*, 905–908.

62. Pizzorusso, T., Medini, P., Berardi, N., Chierzi, S., Fawcett, J.W., and Maffei, L. (2002). Reactivation of ocular dominance plasticity in the adult visual cortex. Science *298*, 1248–1251.

63. Murase, S., Lantz, C.L., and Quinlan, E.M. (2017). Light Reintroduction after Dark Exposure Reactivates Plasticity in Adults via Perisynaptic Activation of MMP-9. Elife *6*.

64. Villalobos, C.A., Wu, Q., Lee, P.H., May, P.J., and Basso, M.A. (2018). Parvalbumin and GABA Microcircuits in the Mouse Superior Colliculus. Front. Neural Circuits *12*, 35.

65. Shang, C., Liu, Z., Chen, Z., Shi, Y., Wang, Q., Liu, S., Li, D., and Cao, P. (2015). BRAIN CIRCUITS. A parvalbumin-positive excitatory visual pathway to trigger fear responses in mice. Science *348*, 1472–1477.

66. Fazzari, P., Paternain, A.V., Valiente, M., Pla, R., Luján, R., Lloyd, K., Lerma, J., Marín, O., and Rico, B. (2010). Control of cortical GABA circuitry development by Nrg1 and ErbB4 signalling. Nature *464*, 1376–1380.

67. Gu, Y., Tran, T., Murase, S., Borrell, A., Kirkwood, A., and Quinlan, E.M. (2016). Neuregulin-Dependent Regulation of Fast-Spiking Interneuron Excitability Controls the Timing of the Critical Period. J. Neurosci. *36*, 10285–10295.

68. Sun, Y., Ikrar, T., Davis, M.F., Gong, N., Zheng, X., Luo, Z.D., Lai, C., Mei, L., Holmes, T.C., Gandhi, S.P., and Xu, X. (2016). Neuregulin-1/ErbB4 Signaling Regulates Visual Cortical Plasticity. Neuron *92*, 160–173.

69. Matta, J.A., Ashby, M.C., Sanz-Clemente, A., Roche, K.W., and Isaac, J.T.R. (2011). mGluR5 and NMDA receptors drive the experience- and activity-dependent NMDA receptor NR2B to NR2A subunit switch. Neuron *70*, 339–351.

70. Sans, N.A., Montcouquiol, M.E., and Raymond, J. (2000). Postnatal developmental changes in AMPA and NMDA receptors in the rat vestibular nuclei. Brain Res. Dev. Brain Res. *123*, 41–52.

71. Paoletti, P., Bellone, C., and Zhou, Q. (2013). NMDA receptor subunit diversity: impact on receptor properties, synaptic plasticity and disease. Nat. Rev. Neurosci. *14*, 383–400.

72. Monyer, H., Burnashev, N., Laurie, D.J., Sakmann, B., and Seeburg, P.H. (1994). Developmental and regional expression in the rat brain and functional properties of four NMDA receptors. Neuron *12*, 529–540.

73. Xing, G.G., Wang, R., Yang, B., and Zhang, D. (2006). Postnatal switching of NMDA receptor subunits from NR2B to NR2A in rat facial motor neurons. Eur. J. Neurosci. *24*, 2987–2992.

74. Sheng, M., Cummings, J., Roldan, L.A., Jan, Y.N., and Jan, L.Y. (1994). Changing subunit composition of heteromeric NMDA receptors during development of rat cortex. Nature *368*, 144–147.

75. Quinlan, E.M., Philpot, B.D., Huganir, R.L., and Bear, M.F. (1999). Rapid, experience-dependent expression of synaptic NMDA receptors in visual cortex in vivo. Nat. Neurosci. *2*, 352–357.

76. Lu, W., and Constantine-Paton, M. (2004). Eye opening rapidly induces synaptic potentiation and refinement. Neuron *43*, 237–249.

77. Hoy, J.L., Bishop, H.I., and Niell, C.M. (2019). Defined Cell Types in Superior Colliculus Make Distinct Contributions to Prey Capture Behavior in the Mouse. Curr. Biol. *29*, 4130–4138.e5.

78. Johnson, K.P., Fitzpatrick, M.J., Zhao, L., Wang, B., McCracken, S., Williams, P.R., and Kerschensteiner, D. (2021). Cell-type-specific binocular vision guides predation in mice. Neuron *109*, 1527–1539.e4.

79. Su, J., Sabbagh, U., Liang, Y., Olejníková, L., Dixon, K.G., Russell, A.L., Chen, J., Pan, Y.A., Triplett, J.W., and Fox, M.A. (2021). A cell-ECM mechanism for connecting the ipsilateral eye to the brain. Proc. Natl. Acad. Sci. USA *118*, e2104343118.

80. Zhao, Z.D., Chen, Z., Xiang, X., Hu, M., Xie, H., Jia, X., Cai, F., Cui, Y., Chen, Z., Qian, L., et al. (2019). Zona incerta GABAergic neurons integrate prey-related sensory signals and induce an appetitive drive to promote hunting. Nat. Neurosci. *22*, 921–932.

81. Furigo, I.C., de Oliveira, W.F., de Oliveira, A.R., Comoli, E., Baldo, M.V.C., Mota-Ortiz, S.R., and Canteras, N.S. (2010). The role of the superior colliculus in predatory hunting. Neuroscience *165*, 1–15.

82. Hoy, J.L., Yavorska, I., Wehr, M., and Niell, C.M. (2016). Vision Drives Accurate Approach Behavior during Prey Capture in Laboratory Mice. Curr. Biol. *26*, 3046–3052.

83. Chalupa, L.M., and Rhoades, R.W. (1977). Responses of visual, somatosensory, and auditory neurones in the golden hamster's superior colliculus. J. Physiol. *270*, 595–626.

84. Fu, J., Tanabe, S., and Cang, J. (2023). Widespread and Multifaceted Binocular Integration in the Mouse Primary Visual Cortex. J. Neurosci. *43*, 6495–6507.

85. De Franceschi, G., and Solomon, S.G. (2018). Visual response properties of neurons in the superficial layers of the superior colliculus of awake mouse. J. Physiol. *596*, 6307–6332.

86. Frenkel, M.Y., and Bear, M.F. (2004). How monocular deprivation shifts ocular dominance in visual cortex of young mice. Neuron *44*, 917–923.

87. Kirkwood, A., Silva, A., and Bear, M.F. (1997). Age-dependent decrease of synaptic plasticity in the neocortex of alphaCaMKII mutant mice. Proc. Natl. Acad. Sci. USA *94*, 3380–3383.

88. Fagiolini, M., Pizzorusso, T., Berardi, N., Domenici, L., and Maffei, L. (1994). Functional postnatal development of the rat primary visual cortex and the role of visual experience: dark rearing and monocular deprivation. Vision Res. *34*, 709–720.

89. Shatz, C.J., and Stryker, M.P. (1978). Ocular dominance in layer IV of the cat's visual cortex and the effects of monocular deprivation. J. Physiol. *281*, 267–283.

90. Olson, C.R., and Freeman, R.D. (1980). Profile of the sensitive period for monocular deprivation in kittens. Exp. Brain Res. *39*, 17–21.

91. Lachica, E.A., Crooks, M.W., and Casagrande, V.A. (1990). Effects of monocular deprivation on the morphology of retinogeniculate axon arbors in a primate. J. Comp. Neurol. *296*, 303–323.

92. Grutzendler, J., Kasthuri, N., and Gan, W.B. (2002). Long-term dendritic spine stability in the adult cortex. Nature *420*, 812–816.

93. Hubel, D.H., Wiesel, T.N., and LeVay, S. (1977). Plasticity of ocular dominance columns in monkey striate cortex. Philos. Trans. R. Soc. Lond. B Biol. Sci. *278*, 377–409.

94. Lendvai, B., Stern, E.A., Chen, B., and Svoboda, K. (2000). Experience-dependent plasticity of dendritic spines in the developing rat barrel cortex in vivo. Nature *404*, 876–881.

95. Dunaevsky, A., Tashiro, A., Majewska, A., Mason, C., and Yuste, R. (1999). Developmental regulation of spine motility in the mammalian central nervous system. Proc. Natl. Acad. Sci. USA *96*, 13438–13443.

96. Wang, L., Sarnaik, R., Rangarajan, K., Liu, X., and Cang, J. (2010). Visual receptive field properties of neurons in the superficial superior colliculus of the mouse. J. Neurosci. *30*, 16573–16584.

97. Cull-Candy, S., Brickley, S., and Farrant, M. (2001). NMDA receptor subunits: diversity, development and disease. Curr. Opin. Neurobiol. *11*, 327–335.

98. Cho, K.K.A., Khibnik, L., Philpot, B.D., and Bear, M.F. (2009). The ratio of NR2A/B NMDA receptor subunits determines the qualities of ocular dominance plasticity in visual cortex. Proc. Natl. Acad. Sci. USA *106*, 5377–5382.

99. Kirkwood, A., Rioult, M.C., and Bear, M.F. (1996). Experience-dependent modification of synaptic plasticity in visual cortex. Nature *381*, 526–528.

100. Ahmadlou, M., Tafreshiha, A., and Heimel, J.A. (2017). Visual Cortex Limits Pop-Out in the Superior Colliculus of Awake Mice. Cereb. Cortex *27*, 5772–5783.

101. Hoffmann, K.P., and Straschill, M. (1971). Influences of cortico-tectal and intertectal connections on visual responses in the cat's superior colliculus. Exp. Brain Res. *12*, 120–131.

102. Rizzolatti, G., Tradardi, V., and Camarda, R. (1970). Unit responses to visual stimuli in the cat's superior colliculus after removal of the visual cortex. Brain Res. *24*, 336–339.

103. Wickelgren, B.G., and Sterling, P. (1969). Influence of visual cortex on receptive fields in the superior colliculus of the cat. J. Neurophysiol. *32*, 16–23.

104. Rodman, H.R., Gross, C.G., and Albright, T.D. (1990). Afferent basis of visual response properties in area MT of the macaque. II. Effects of superior colliculus removal. J. Neurosci. *10*, 1154–1164.

105. Ogasawara, K., McHaffie, J.G., and Stein, B.E. (1984). Two visual corticotectal systems in cat. J. Neurophysiol. *52*, 1226–1245.

106. Illing, R.B., Vogt, D.M., and Spatz, W.B. (1990). Parvalbumin in rat superior colliculus. Neurosci. Lett. *120*, 197–200.

107. Behan, M., Steinhacker, K., Jeffrey-Borger, S., and Meredith, M.A. (2002). Chemoarchitecture of GABAergic neurons in the ferret superior colliculus. J. Comp. Neurol. *452*, 334–359.

108. González-Soriano, J., González-Flores, M.L., Contreras-Rodríguez, J., Rodríguez-Veiga, E., and Martínez-Sainz, P. (2000). Calbindin D28k and parvalbumin immunoreactivity in the rabbit superior colliculus: an anatomical study. Anat. Rec. *259*, 334–346.

109. Pizzorusso, T., Medini, P., Landi, S., Baldini, S., Berardi, N., and Maffei, L. (2006). Structural and functional recovery from early monocular deprivation in adult rats. Proc. Natl. Acad. Sci. USA *103*, 8517–8522.

110. Orlando, C., Ster, J., Gerber, U., Fawcett, J.W., and Raineteau, O. (2012). Perisynaptic chondroitin sulfate proteoglycans restrict structural plasticity in an integrin-dependent manner. J. Neurosci. *32*, 18009–18017. 18017a.

111. Shang, C., Chen, Z., Liu, A., Li, Y., Zhang, J., Qu, B., Yan, F., Zhang, Y., Liu, W., Liu, Z., et al. (2018). Divergent midbrain circuits orchestrate escape and freezing responses to looming stimuli in mice. Nat. Commun. *9*, 1232.

112. Shang, C., Liu, A., Li, D., Xie, Z., Chen, Z., Huang, M., Li, Y., Wang, Y., Shen, W.L., and Cao, P. (2019). A subcortical excitatory circuit for sensory-triggered predatory hunting in mice. Nat. Neurosci. *22*, 909–920.

113. Hong, Y.K., Kim, I.J., and Sanes, J.R. (2011). Stereotyped axonal arbors of retinal ganglion cell subsets in the mouse superior colliculus. J. Comp. Neurol. *519*, 1691–1711.

114. Yu, H., Xiang, X., Chen, Z., Wang, X., Dai, J., Wang, X., Huang, P., Zhao, Z.D., Shen, W.L., and Li, H. (2021). Periaqueductal gray neurons encode the sequential motor program in hunting behavior of mice. Nat. Commun. *12*, 6523.

115. Huang, L., Yuan, T., Tan, M., Xi, Y., Hu, Y., Tao, Q., Zhao, Z., Zheng, J., Han, Y., Xu, F., et al. (2017). A retinoraphe projection regulates serotonergic activity and looming-evoked defensive behaviour. Nat. Commun. *8*, 14908.

116. Wang, F., Li, E., De, L., Wu, Q., and Zhang, Y. (2021). OFF-transient alpha RGCs mediate looming triggered innate defensive response. Curr. Biol. *31*, 2263–2273.e3.

117. Červený, J., Begall, S., Koubek, P., Nováková, P., and Burda, H. (2011). Directional preference may enhance hunting accuracy in foraging foxes. Biol. Lett. *7*, 355–357.

118. Chou, L.M., Leong, C.F., and Choo, B.L. (1988). The role of optic, auditory and olfactory senses in prey hunting by two species of geckos. J. Herpetol. *22*, 349–351.

119. Hughes, N.K., Price, C.J., and Banks, P.B. (2010). Predators are attracted to the olfactory signals of prey. PLoS One *5*, e13114.

120. Ylönen, H., Sundell, J., Tiilikainen, R., Eccard, J.A., and Horne, T. (2003). Weasels'(Mustela nivalis nivalis) preference for olfactory cues of the vole (Clethrionomys glareolus). Ecology *84*, 1447–1452.

121. Togunov, R.R., Derocher, A.E., and Lunn, N.J. (2017). Windscapes and olfactory foraging in a large carnivore. Sci. Rep. *7*, 46332–46410.

122. Rushworth, M.F.S., Noonan, M.P., Boorman, E.D., Walton, M.E., and Behrens, T.E. (2011). Frontal cortex and reward-guided learning and decision-making. Neuron *70*, 1054–1069.

123. Rossier, D., La Franca, V., Salemi, T., Natale, S., and Gross, C.T. (2021). A neural circuit for competing approach and defense underlying prey capture. Proc. Natl. Acad. Sci. USA *118*, e2013411118.

124. Goodroe, S.C., and Spiers, H.J. (2022). Extending neural systems for navigation to hunting behavior. Curr. Opin. Neurobiol. *73*, 102545.

125. Kaplan, R., King, J., Koster, R., Penny, W.D., Burgess, N., and Friston, K.J. (2017). The neural representation of prospective choice during spatial planning and decisions. PLoS Biol. *15*, e1002588.

126. Howard, L.R., Javadi, A.H., Yu, Y., Mill, R.D., Morrison, L.C., Knight, R., Loftus, M.M., Staskute, L., and Spiers, H.J. (2014). The hippocampus and entorhinal cortex encode the path and Euclidean distances to goals during navigation. Curr. Biol. *24*, 1331–1340.

127. Javadi, A.H., Patai, E.Z., Marin-Garcia, E., Margois, A., Tan, H.R.M., Kumaran, D., Nardini, M., Penny, W., Duzel, E., Dayan, P., and Spiers, H.J. (2019). Backtracking during navigation is correlated with enhanced anterior cingulate activity and suppression of alpha oscillations and the 'default-mode' network. Proc. Biol. Sci. *286*, 20191016.

128. Chan, J., Hao, X., Liu, Q., Cang, J., and Gu, Y. (2021). Closing the Critical Period Is Required for the Maturation of Binocular Integration in Mouse Primary Visual Cortex. Front. Cell. Neurosci. *15*, 749265.

129. Cheng, C., Trzcinski, O., and Doering, L.C. (2014). Fluorescent labeling of dendritic spines in cell cultures with the carbocyanine dye "DiI. Front. Neuroanat. *8*, 30.

130. Haber, M., Zhou, L., and Murai, K.K. (2006). Cooperative astrocyte and dendritic spine dynamics at hippocampal excitatory synapses. J. Neurosci. *26*, 8881–8891.

STAR★METHODS

KEY RESOURCES TABLE

REAGENT or RESOURCE	SOURCE	IDENTIFIER
Antibodies		
Rabbit monoclonal anti- Parvalbumin	Cell Signaling Technology	Cat# 80561S
wisteria floribunda agglutinin	Sigma	L1516
Mouse monoclonal anti-GABA	Sigma	Cat# A0310
Alexa Fluor 594	Abcam	Cat# ab150080
Alexa Fluor 647	Abcam	Cat# ab150115
FITC-conjugated Streptavidin	Sangon	Cat# D110512
NR2A	Abclonal	Cat# A0924
NR2B	Abclonal	Cat# A3056
GAPDH	Abclonal	Cat# AC002
Anti-rabbit IgG HRP-linked Antibody	Cell Signaling Technology	Cat# 7074S
Anti-Mouse IgG HRP-linked Antibody	Abclonal	Cat# AS003
DAPI	Solarbio	Cat# C0065
Chemicals, peptides, and recombinant proteins		
Cholera toxin subunit B 488	Invitrogen	Cat# C34775
Cholera toxin subunit B 594	Invitrogen	Cat# C34777
DiI	Thermo Fisher Scientific	Cat# D282
Muscimol	Bio-Techne	Cat# 0289/10
TNC 201	MCE	Cat# HY-13457
Ro 25-6981	Abcam	Cat# ab120290
CPP	Abcam	Cat# ab120160
NMDA	Sigma	Cat# M3262
Critical commercial assays		
Pierce Rapid Gold BCA Kit	Beyotime	Cat# P0010
Nissl Stain Kit	Solarbio	Cat# G1430
Experimental models: Organisms/strains		
Mouse: C57BL/67	Jackson Laboratory	Stock No: 000664
Software and algorithms		
GraphPad Prism version 8	GraphPad Software, San Diego, CA, USA	https://www.graphpad.com/
Imaris ×64 software version 8.1.2	Oxford Instruments	https://imaris.oxinst.cn/
Adobe Illustrator CC	Adobe	https://www.adobe.com/products/illustrator.html
ImageJ	NIH	https://imagej.net/software/imagej
Python software 3.9.8	Python	https://www.python.org/
Psychopy	Psychopy	https://www.psychopy.org/
Neuroexplorer	Plexon	https://plexon.com/products/neuroexplorer/
Offline Sorter v4.0	Plexon Inc	https://plexon.com/offline-sorter-v-4-4-0/

RESOURCE AVAILABILITY

Lead contact

Further information and requests for resources and reagents should be directed to and will be fulfilled by the lead contact, Dr. Yu Gu (guyu_@fudan.edu.cn).

Materials availability

All unique/stable reagents generated in this study are available from the lead contact with a completed Materials Transfer Agreement.

Data and code availability

(1) All original data reported in this paper are available from the lead contact upon request.
(2) This paper does not report the original code.
(3) Any additional information required to reanalyze the data reported in this paper is available from the lead contact upon request.

EXPERIMENTAL MODEL AND SUBJECT PARTICIPANT DETAILS

Animals

Wild-type (male and female C57BL/6J randomly) mice were used in this study, aged P13, 21, 22, 28, 32, 33 and 60. All mice were housed at a constant temperature (24°C) with *ad libitum* access to a standard rodent diet under a 12 h:12 h light/dark cycle (~200 lux white ambient illumination for light cycle). All efforts were made to minimize animal discomfort. All animal procedures were approved by the Institutional Animal Care and Use Committee of Fudan University and the Institutional Animal Care and Use Committee of Tianjin Medical University.

METHOD DETAILS

Monocular deprivation

Mice of various ages were anesthetized with isoflurane (RWD Life Science, Shenzhen) in the air (4% for induction, 1–2% for maintenance). The area immediately surrounding the eye to be sutured was wiped with saline. The upper and lower lid margins were trimmed, and the eye was flushed with saline. An antibiotic ointment (CISEN, Wenshang) was applied to the eye to decrease the incidence of postoperative infection and inflammation. Three to four mattress sutures were performed using 6-0 silk (Lingqiao, Ningbo), opposing the full extent of the trimmed lids. Animals were recovered by placing them on a heating pad maintained at 37°C through a feedback rectal thermo probe (Harvard Apparatus, USA) and returned to their cages when fully alert and mobile. Animals were checked daily to make sure that their eyes remained closed and uninfected. Only animals whose lid fusions remained intact throughout the 4d period or long-term monocular deprivation (LTMD, 8 days) were considered in the results, whereas mice with scarring of the cornea and signs of infection were excluded from the study. Control animals are littermates that went through surgery with upper and lower lid margins trimmed but not sutured.

Cannula injection

Mice were placed in a plastic chamber, anesthetized with isoflurane in the air (5% for induction, 1–2% for maintenance), and then restrained in a stereotaxic apparatus (RWD Life Science, Shenzhen), and their scalp was shaved and disinfected with 75% ethanol. Artificial tear (HYLO, Germany) was used to protect the eyes of the animals from drying during surgery. A skull drill was used to perform two small craniotomies above the bilateral SC (AP, −3.5 to −3.9mm; ML, ±0.5 to 1.0 mm, DV, −1.0 to −1.6 mm), and a 27G stainless-steel cannula with a plastic cup (RWD Life Science, Shenzhen) was affixed to the bone using dental cement (LELE, Shanghai). A matched obturator cap was used to seal the cannula. The animals were then maintained at approximately 37°C on an electric heating blanket and housed separately until complete recovery from anesthesia. Animals were allowed to recover for at least 3 days before infusions. An osmotic pump (Longer Pump, Longer Precision Pump Co., Ltd.) was connected to the cannula through a syringe. CPP (1.5μL/side, Abcam, ab120160, 2 mg/mL diluted with ACSF solution)/TCN201(2μL/side, MCE, HY-13457, 100μM diluted with ACSF solution)/Ro25-6981(2μL/side, Abcam, ab120290, 0.88 mM diluted with ACSF solution)/hyaluronidase (Hya, 2μL/side, Sigma-Aldrich, H-1136, 200 U/mL diluted with PBS solution) was daily injected via an osmotic pump into bilateral SC at 750 nL/min. After the injection, the syringe remained in the brain for 10 min to allow for diffusion of the drug. Before the behavior test and *in vivo* electrophysiology, the cannula was carefully removed to prevent conflict with the following manipulations.

Stereotaxic injection

Mice were anesthetized with isoflurane as aforementioned and restrained on a stereotaxic apparatus (RWD Life Science, Shenzhen) by nose clip and ear bars. Erythromycin ointment (Guangdong Hengjian Pharmaceutical Co., Ltd) was applied to keep the corneal moist. The scalp was shaved and cleaned, and then a linear incision on the skin was made to expose the skull, which was subsequently cleaned with a cotton swab dipped in PBS. The brain was adjusted to be flat in both x and y coordinates. According to "The Mouse Brain" (Keith B.J. Franklin and George Paxinos, the third edition, Elsevier), bregma was defined as the origin of stereotaxic with $x = 0, y = 0, z = 0$, and lambda was defined as $x = 0, y = -4.2$ mm, $z = 0$. Injection coordinates for SC were $x = 0.5$ to 1.0 mm, $y = -3.5$ to -3.9 mm, $z = -1.0$ to -1.6 mm, for V1 were $x = 2.6$ to 3.1 mm, $y = -3.4$ to -4.0 mm, $z = -0.4$ to -0.6 mm. If the distance between bregma and lambda was not 4.2 mm, the coordinates for the injection site were calculated proportionally. The skull above the target area was drilled open and a glass pipette (WPI, pulled by Sutter P97) was inserted into the injection site. 150-200nL cholera toxin subunit B 594 (CTB594, Invitrogen, C34777, 1 μg/μL) was unilaterally injected into SC, and 200nL *N*-methyl-*d*-aspartic acid (NMDA, Sigma-Aldrich, M326) was bilaterally injected into V1 or SC at the rate of 0.5 nL/s for each site. 1 injection site for

CTB594 and 6 injection sites for NMDA were randomly chosen within the area for each hemisphere. After injection, the glass pipette was pulled out slowly for 10 min. CTB594 injected mice were perfused and brains were fixed with 4% PFA 4 days later, sliced on a vibratome machine (Leica, VT 1000S) at a thickness of 100μm and imaged with fluorescent microscopy (Nikon Eclipse Ni). NMDA-injected mice were put back into the home cage and followed by a behavior test.

Eye injection

Borosilicate glass microcapillaries were made into injection needles with a tip diameter of 5–10 μm using a P-97 micropipette puller (Sutter Instrument, USA). The tip was beveled with an EG-401 micropipette grinder (Narishige Group, Japan). The injection needles were filled with paraffin oil and mounted on a microsyringe (RWD Life Science, Shenzhen), and 2μL of CTB488 (Invitrogen, 1 μg/μL, in 0.01M PBS) was then drawn up into the needle. Mice were anesthetized with isoflurane (RWD Life Science, Shenzhen) in the air (4% for induction, 1–2% for maintenance). To prevent corneal drying, 0.3% sodium hyaluronate eye drops (one drop every 5 min) were applied to the eyes while the animals were anesthetized and during the intravitreal injection. One drop of proparacaine was instilled into each eye to block local reflexes, and the depth of anesthesia was confirmed by gently touching the conjunctiva 1–2 min later. After the conjunctival reflex disappeared, the mouse was placed under the microscope, and the conjunctiva below the corneal limbus was clamped with forceps to make the eyeball protrude out of the orbit, and the equatorial plane of the eyeball was kept in a horizontal and stable state. Then the position and the angle of the needle tip were adjusted to make the needle tip form an angle of 30° with the equatorial plane of the eyeball. The needle tip was then carefully and slowly inserted through the sclera into the vitreous cavity of the mouse, avoiding piercing the lens, and a total of 1035 nL of CTB488 (69 nL once, 15 times in total) was finally injected with a syringe pump (Legato 130, KD Scientific, USA) into the vitreous of the left eye. After injection, the needle was left in the vitreous cavity for 1min to prevent liquid leakage, and then slowly removed. The eye was gently returned to the socket by closing the eyelids, tobramycin ointment was then applied to the cornea and the injection area. CTB594 (Invitrogen, 1 μg/μL, in 0.01M PBS) was drawn up into a new needle with another microsyringe and the injection was conducted in the right eye in the same way. After the injection, the mice were placed on a heating pad for complete recovery before being transferred back to their home cage. After 4d period of habituation, CTB488 and CTB594 injected mice were perfused and brains were fixed with 4% PFA for 18 h at 4°C. The brains were then mounted on a vibratome machine (Leica, VT 1000S) sliced coronally at a thickness of 100μm and imaged with confocal microscopy (Leica, SP8 SR). High-resolution images on the same plane were combined with Leica Application Suite X (Leica Microsystems, USA). For each animal, all the analyzed high-resolution combined images were from 4 coronal slices in the anteroposterior coordinate of AP -3.5 to −3.8mm. Images were background subtracted. The value of 3 standard deviations above the mean gray value in a non-labeled brain region of the analyzed channel was used as background. The regions of interest (ROIs) were confined in the superficial superior colliculus (sSC). The borders of the sSC were outlined manually according to the fluorescence signals of both channels. Thus, the ROI in the ipsilateral hemisphere of the SC for the retinal input from the right eye/deprived eye can still be accurately selected. The mean gray values of the analyzed channel in the ROIs of each hemisphere of the SC were used for statistical analysis. The measurements of 4 slices were averaged for each animal. The averaged mean gray values were compared between the Ctrl group and the MD group for each postnatal age.

In vivo electrophysiology

Mice were anesthetized with an intraperitoneal injection of urethane (1–1.25 g/kg, diluted to 10% in saline solution, Sigma-Aldrich) and then sedated with chlorprothixene (Abcam, ab143077, 5 mg/kg in DMSO, *i.m*). The suture was removed with fine scissors and examined under a stereomicroscope before electrophysiological recordings. The skin covering the scalp was removed to expose the skull. A metal head plate was implanted on top of the skull with Super-Bond (C&B, Japan), and the plate was then mounted to a stand on the vibration isolation table. Both contralateral and ipsilateral eyes were treated with a thin layer of silicone oil to prevent dehydration. A small craniotomy (~2 mm^2) was made on the skull to expose SC (craniotomy centers for most recordings: AP, −3.8 mm; ML, +0.5 mm; for recordings in the anterior portion of the SC: AP, −3.4mm; ML, +0.5 mm; for recordings in the middle and lateral portion of the SC: AP, −4.1mm; ML, +1.2 mm; for recordings in the posterior portion of the SC: AP, −4.7mm; ML, +0.5 mm; expanded recordings were made for mapping the distribution of binocular cells throughout the SC, but no recording was made for the portion of the SC below the area covered by the venous sinus) or binocular V1 (V1b, AP, −4.0 mm; ML, +3.0 mm). Probes were coated in 1,1′-dioctadecyl-3,3,3′,3′-tetramethylindocarbocyanine percolate (DiI, Thermo Fisher Scientific, D282) for post-procedure visualization of probe placement. Penetration depth measured by distance from the pia in re-constructions was well-matched to the estimates obtained from the distance traveled in the micromanipulator. The exposed brain was kept moist with ACSF. Throughout recordings, the toe-pinch reflex was monitored and additional urethane (5%) was supplemented if necessary. The animal's temperature was maintained at 37°C on a heating pad (Harvard Apparatus, USA) on which the animal rested throughout the experiment. For drug administration (CPP/TCN201/Ro25-6981/Hya) experiments, all recordings were performed from the trajectory of cannula implantation.

During recording, silicon probes (16 channels, ASSY-1-16-1, Lotus Biochips, USA) were inserted perpendicular to the pial surface. Recording sites were 1000–1500 μm below the pial surface for SC and 400–600 μm for V1. V1 was left intact during the SC recordings. For each animal, 5–10 penetrations were made and cells recorded across all depths were included in our recordings. For the muscimol (5mM, Bio-Techne) administration experiment, to ascertain single units were recorded specifically from the deep layers of

V1, only recordings made at depths of more than 500μm were included in this study, and the depths were confirmed for a subset of recordings by subsequent DiI staining and penetration re-construction.

Visual stimuli

Stimuli were presented using an LCD monitor (40 × 40 cm, 60 Hz refresh rate, 100% contrast, ~35-45 cd/m^2 luminance) placed 20 cm in front of the animal. Sinusoidal gratings drifting perpendicular to their orientations were generated with the PsychoPy (v3.00) package. The direction of the gratings varied between 0° and 330° (12 steps at 30° spacing) in a pseudorandom sequence. The spatial frequency of the stimuli was set at 0.04 cycle/degree while the temporal frequency at 2 Hz. Each stimulus was presented for 1.5 s, with a 1.5 s inter-stimulus gray screen interval to determine the spontaneous firing rate. To calculate the visually-evoked spiking response, the spontaneous spiking rate was subtracted from the total rate at each stimulus condition. For each recording session, the sequence was repeated for at least 5 trials in a pseudorandom order in two different ocular conditions: monocularly to the eye contralateral to the recording site, and monocularly to the ipsilateral eye. For monocular conditions, an opaque piece of cardboard was placed directly in front of the opposite eye to prevent it from viewing the screen. For each identified unit, we determined if the unit was visually responsive under each ocular condition. A unit was determined to be visually responsive if 1) the response to the preferred stimulus was significantly different from the spontaneous rate based on a one-way ANOVA comparing the spontaneous rate and responses to all orientations shown at the preferred, 2) the mean firing rate elicited by the preferred stimulus was greater than 2 standard deviations above the spontaneous rate of the unit, 3) the firing rate elicited by the preferred stimulus was greater than 2 standard deviations above the spontaneous rate in at least two-thirds of the trial. Units that were determined to be visually responsive under any ocular condition were utilized for further analysis. At the end of each session, both eyes were occluded to make sure the cardboard was indeed opaque.

Spike detection and sorting

The recorded data from the electric activity of neurons were exported to and analyzed via an offline sorter software(v4.0) (Plexon Inc., Dallas, TX) as described before.[128] Spikes were detected through manual amplitude threshold discrimination, with a waveform length of 800μs, threshold period of 200μs, and dead time of 800μs. The threshold value was assigned two times the standard deviations of the amplitude of background activity. Waveforms with uncharacteristic shapes, such as those caused by stimulus or movement artifacts and an abnormal Inter Spike Interval (ISI<1ms) will be excluded in this procedure for subsequent analysis. Next, spike sorting was performed to classify the electric activity of single units based on principal component analysis which was performed to score spikes with a high degree of similarity in a 3D feature space, then with Semi-Automatic Clustering using the best algorithm (K-Means, Standard E-M, etc.). Finally, spike clusters with a minimum evoked firing rate >3 spikes/s to at least one stimulus direction were defined as clear contralateral or ipsilateral responses, and all the data of these units were saved for further analysis. NeuroExplorer (version 5.23, Nex Technologies, Colorado Springs) was used to analyze the firing activity of clusters of neurons. The quality of sorted data was validated through auto-correlogram analysis because it displays a single spike train against itself. Another tool that compares the arrival times of spike trains is a cross-correlogram. Through cross-correlogram, the different identified clusters of spikes were explored to validate the exact number of neurons in each set of recorded data. Finally, the average firing rate histograms were generated and verified for all neurons, over the entire period of the recording session.

Electrophysiological data analysis

SC binocular neurons were assigned OD scores according to the methods of the Hubel and Wiesel classification system with some modifications.[5,62] Optimal stimuli were presented to either eye alternately, and the relative strength of the response was determined. Cells were assigned an OD score of 1 if the contralateral versus ipsilateral response ratio (C/I) was >10 and 7 if C/I < 0.1. Cells responding equally well to stimuli presented to either eye (0.667 < C/I < 1.5) were assigned an OD score of 4. OD scores of 2 (3 < C/I < 10) or 3 (1.5 < C/I < 3) and 5 (0.333 < C/I < 0.667) or 6 (0.1 < C/I < 0.333) were assigned if the cell responded better or was dominated by response to stimuli presented to the contralateral and ipsilateral eye, respectively. Only cells with clear ipsilateral response were considered in the results. The contralateral bias index (CBI) was calculated according to the formula:

$$CBI = [(n1-n7) + (2/3)\,(n2-n6) + (1/3)\,(n3-n5) + N] / 2N,$$

where N = total number of cells and nx = number of cells with OD scores equal to x.

For mapping the distribution of binocular cells throughout the SC, the ocular dominance index (ODI) was used to assess the binocularity of the SC neurons. The ODI was calculated according to the formula: ODI = (C-I)/(C + I), where C and I represent the response magnitude to the contralateral and ipsilateral eyes, respectively. The proportion of binocular cells in each SC location was defined as the ratio of the number of binocularly responsive cells to the number of all recorded visually responsive cells at the location.

DiI staining

Dendritic spines were visualized using a fluorescent lipophilic dye, DiI (Thermo Fisher Scientific, D282),[129,130] which exhibits high photostability and prominent fluorescence, thus serving as an effective means of illuminating the morphological dendritic arborizations and spines. Mice were deeply anesthetized with an overdose of isoflurane and immediately perfused intracardially with saline followed by cold 1.5% paraformaldehyde (PFA) in 0.1 M phosphate buffer (pH 7.4). The brain was dissected carefully and postfixed in

the same fixative for 2 h at 4°C. The brain was sliced for 100 μm thick with Leica vibratome and then collected on glass slides. The sonicated fine powdered DiI was placed gently with the aid of a thin histological needle. The exposed tissue sections on glass slides covered with PBS were kept at room temperature for approximately 16 h in the dark. PBS was removed before the final fixation of the tissue with 4% paraformaldehyde in PBS for 30 min. The slices were washed with PBS for 10 min twice and mounted under a coverslip with anti-fading non-diluted mounting media. To prevent the mounting media from drying, the borders of the coverslip were sealed with fast-drying nail polish. The dendrites of interest (predominantly focusing on the anterior-medial crescent of SC) can be visualized and reconstructed by adding the z stack of images using the Nikon software.

Perineuronal nets staining

To stain perineuronal nets (PNNs), free-floating sections were washed in PBS 3 times and incubated for 2 h in a blocking solution (3% BSA in PBS for WFA staining) at RT. The sections were then incubated overnight at 4°C with Lectin from Wisteria floribunda (WFA 1:200, Sigma), a lectin that recognizes most N-acetylgalactosamine residues present in PNNs. After primary antibody incubation, the sections were washed in PBS followed by secondary antibody incubation with FITC-labeled streptavidin (1:200, Sangon Biotech). Each staining round was accompanied by nuclear counterstaining with 4′,6-diamidino-2-phenylindole (DAPI 1:1,000, Solarbio) in PBS. All slides were mounted with anti-fading Fluoromount (Sigma, F4680) and left at 4°C in a dark chamber until imaging. The brain sections were acquired using identical parameters with fluorescent microscopy (Nikon Eclipse Ni), SC and V1b were identified according to Mouse Brain Atlas (Keith B.J. Franklin and George Paxinos, the third edition, Elsevier). 5 z sections were stacked for each image, exported as TIFF files. The number of WFA-positive neurons in the V1 binocular zone was counted by ImageJ in an area of 500 × 550 μm, and SC in an area of 850 × 700 μm. The average cell density of each mouse was compared between the experimental groups.

Immunohistochemistry

Mice were anesthetized with an overdose of isoflurane and immediately perfused intracardially with saline followed by ice-cold 4% paraformaldehyde (PFA) in 0.1 M phosphate buffer (pH 7.4). Brains were dissected and postfixed in the same fixative overnight at 4°C, followed by equilibration in 30% sucrose in PBS for over 48 h. The 30 μm thick coronal sections were made in a cryostat and then stored at −80°C. To stain PV, GABA, and NRG1, the rabbit polyclonal antibody against PV, the mouse monoclonal antibody against GABA, and the mouse monoclonal antibody against NRG1 were used (PV, 1:1000, Swant; GABA, 1:1000, Sigma; NRG1, 1:200, CL488-66492, Proteintech). Sections were first washed three times (10 min for each) in 0.1 M phosphate-buffered saline (1× PBS, pH 7.4), then blocked in 5% normal goat serum (NGS) and 0.3% Triton X-100 (Solarbio, T8200) in PBS for 1 h, and finally incubated in the PBS solution containing primary antibodies overnight at 4°C. After three washes (10 min for each) in PBS, the sections were incubated in PBS containing secondary antibodies for 2 h at room temperature. After three 5-min washes in PBS, sections were incubated in DAPI (Solarbio, C0065) staining solution for 10 min. After another round of three 5-min washings in PBS, the stained sections were mounted onto glass slides, air-dried, and covered slipped with Mounting Medium (Yeasen, 36308ES20).

Nissl staining

Sections mounted on gelatine-coated slides were dehydrated with an ascending series of ethanol, treated with xylene for 5 min, and rehydrated in a descending series of ethanol and MilliQ water. Then, the sections were treated with 1% cresyl violet (Solarbio) solution for 1 h in 56°C followed by differentiation in Nissl Differentiation solution for 2 min. Then, the sections were dehydrated in ascending series of ethanol, treated with xylene, and coverslipped using DPX Mounting medium (Sigma–Aldrich, USA) and visualized with a microscope.

Western blot

The SC of P13, P28, and P60 mice were dissected under deep anesthesia with isoflurane. The bilateral SC of each mouse was mixed as one sample. Proteins were extracted with RIPA lysis buffer containing a complete EDTA-free protein inhibitor cocktail (Roche Applied Science). After blocking in 5% nonfat dry milk (Beyotime, P0216) in 20 mM PBST, the PVDF membranes were incubated with rabbit anti-NR2A (1:2000, ABclonal, A0924) and rabbit anti-NR2B (1:2000, ABclonal, A3056), respectively. Housekeeping proteins were probed with mouse anti-GAPDH (1:2000, ABclonal, AC002) antibodies, followed by the respective HRP-conjugated secondary antibodies (1:2000, CST). The membranes were then developed using SuperSignal West Pico Chemiluminescent Substrate (Tanno, 180-501W). Western blot analysis was repeated multiple times, and the optical density of each band was determined using ImageJ software and normalized to GAPDH.

Predatory hunting

The procedure of the predatory hunting experiment was modified from a published method.[80,112] In brief, all mice used for cricket hunting were singly housed and pre-habituated with crickets for 3 days (2 days with 2.5-g chow restriction, and 1 day *ad libitum*). During the habituation period, six crickets (three young and three adult crickets, purchased from www.taobao.com) were introduced overnight. Before hunting practice or the test, the mice were transferred to the testing room and habituated to the room conditions for 3 h before the experiments started. The arena was cleaned with 70% ethanol to eliminate odor cues from other mice. The mice were let freely explore the cage for 10 min before the experiment, and crickets were gently put in the opposite corner to where the mice

were. Hunting behaviors were measured in a home cage without regular mouse bedding. After entering, the mice were allowed to explore the arena for 10 min, followed by the introduction of a cricket. For each mouse, predatory hunting was repeated for three trials, each trial began with the introduction of prey to the cage. The trial ended when the predator finished ingesting the captured prey, and the cricket debris was removed before beginning a new trial. After the tests, the mice were put back in their home cage.

The counting of time was initiated once the cricket was introduced into the arena. Mouse behavior was recorded in the arena using an overhead camera (50 frames/s, Point Gray Research). The behavioral events were manually analyzed by playing back the recorded videos. We used three parameters (latency to attack, attack duration, and attack frequency) to quantify the efficiency of predatory hunting of mice. All behaviors were scored by the same experimenters, who were blinded to the animal treatments.

QUANTIFICATION AND STATISTICAL ANALYSIS

Statistical analyses were performed using GraphPad Prism software (version 8.3) and custom Python scripts. Parametric unpaired Student's t-test and non-parametric Mann-Whitney test were applied to compare data from different groups of data when needed, while a paired Student's t-test was used for two measurements within the same subject. A one-way ANOVA was used to determine the significance between three or more independent experimental groups, followed by Tukey's post hoc test for pairwise comparisons when ANOVA $p < 0.05$. Data were expressed as mean ± SEM, and significance was placed at $p < 0.05$. *$p < 0.05$, **$p < 0.01$, ***$p < 0.001$ applicable to all figures.